Progress In Electromagnetics Research, PIER 12, 371–419, 1996

ELECTROMAGNETIC SCATTERING BY BURIED OBJECTS IN THE HF/VHF/UHF FREQUENCY BANDS

R. H. Ott

1. Introduction

The electromagnetic scattering by buried objects is complicated by the presence of the air-earth interface. For applications involving radar in the HF/VHF/UHF frequency bands, the air-earth interface is usually rough, defined in extent by the antenna footprint (3-dB beamwidth). Several authors (Hill, 1988, Hill and Cavecy, 1987, and Baum, 1994) have investigated the EM scattering by buried objects when the air-interface is perfectly flat. In this paper, the starting point for the derivation for the scatter by a buried object is Kern's (1981) plane-wave scattering-matrix formulation. Kern's method provides the mathematical foundation for the propagation and scattering of plane

waves in layered media where one or more of the layers contain a scatterer. The method is a powerful means for combining the transmit and receive antenna pattern, the scattering by the buried object, and the effect of the interface including multiple bounces between the target and interface (Hill, 1988). The methods and techniques presented in this paper extend Hill's results in three areas: 1) the derivation of the scattering matrix for an ellipsoidal scatterer as a function of its polarizability, representing it as a dyad for inclusion in the plane-wave spectrum representation, 2) the derivation of the matrices accounting for the multiple reflection between the buried object and the interface, and 3) the inclusion of the EM backscatter from a rough 3-D interface.

Electromagnetic scattering from rough surfaces is an important subject in and of itself. In this paper, the derivation for the EM back scatter from a rough 3-D interface is new in that it uses the dyadic Green's function for the magnetic surface fields. The vector integral equation in terms of the dyadic Green's function is exact provided the surface fields satisfy the boundary conditions. This provides a starting point for the 3-D rough surface scatter in this paper. The formulation employs both the electric and magnetic surface currents on the finitely conducting local tangent plane at the point where the incident wave is specularly reflected with the TE and TM reflection coefficients. For the case of a perfectly conducting surface, the back scatter result agrees with Collin's "New Full Wave Theory" (Collin, 1992), and at grazing the result reduces to the correct perturbation answer (Barrick, 1970, Rice, 1951).

Since the target scatter uses a low-frequency approach, there is an upper frequency limit beyond which the results are not exact. The wavelength in the medium is $\lambda_o/\sqrt{\epsilon_r}$, which at 300 MHz is about 50 cm for sandy soil. The physical size of the scatter in a low-frequency approach is limited in terms of wavelength for the results to be rigorously valid. The use of the Method of Moments (MOM) to solve for the currents on the scatter and then to cast the solution for the currents ($\underline{J}$ and $\underline{K}$) into the expression for the scattered fields in a form which is compatible with Kern's plane-wave spectrum approach is well beyond the scope of this paper. Therefore, even though the low-frequency approximation limits the range for rigorously calculating scattered fields, the low-frequency method is pushed in frequency beyond the strict upper limit to obtain approximate results for the scattered fields from the object. Actually, this approximation may not be as inaccurate as first

believed, since a scatterer usually has edges instead of being entirely smooth. These edges cause the scattered fields to increase as a power of the frequency just as a smooth object does in the Rayleigh region.

All the steps in the mathematical derivations are presented so that the reader will spend less time understanding the analysis and referring to an appendix or a long list of references, containing some of the steps in the approach, and more time of determining the applicability of the assumptions regarding the physics of the detection problem. Also, the analysis presented will determine which frequency band is optimum for detection after applying the associated computer algorithm to several examples of target size, target depth, radar position and frequency band. The application of the computer code to all these possible scenarios is beyond the scope of this paper.

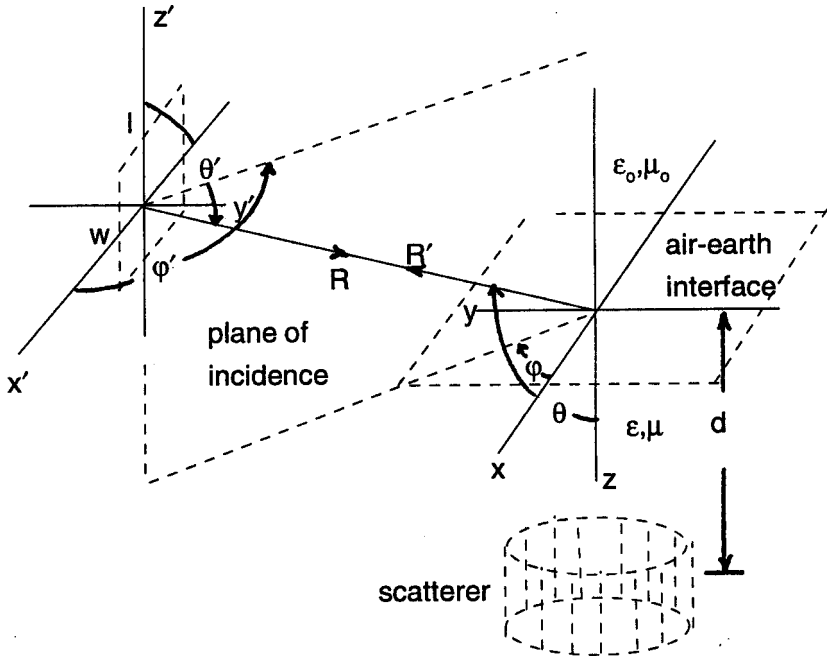

Figure 1. Geometry for a buried object beneath an air-earth interface.

2. Incident Field in Moving Frame

In general, the radar or observer is in a moving in relation to the buried object (e. g., in an unmanned air vehicle, UAV, or a remotely piloted vehcile, RPV). For the geometry in Figure 1, a z-directed dipole would only produce a E_θ component of incident field, and this component would be in the incidence plane. An x-directed dipole in Figure 1 produces both E_θ and E_Φ components of electric field where E_θ is in the plane of incidence (TM polarization) and E_Φ is perpendicular to the plane of incidence (TE polarization). This is true in the far-field where the total field can be represented as a superposition of plane waves. Thus, in general, as the location of the observer in Figure 1 changes, the plane of incidence rotates with respect to the fixed frame on the earth, and both TM and TE components of the incident field are present. This is the case even when the dimension of the vertical aperture, w, in Figure 1 is zero, corresponding to the case of an infinitesimally thin dipole oriented along the x-axis (Lo and Lee, 1993). The derivation of the TM and TE components of the incident field in the moving frame begins with the definition for the vector potential given by

$$\begin{aligned}
\underline{A} &= \underline{e}_x \left(\frac{IL}{4\pi}\right) \frac{e^{ikr'}}{R'} \\
R' &= \sqrt{x'^2 + y'^2 + z'^2} \\
\underline{H} &= \nabla x \underline{A} \cong ik \frac{e^{ikR'}}{R'} \left(\underline{e}_y \frac{z'}{R'} - \underline{e}_z \frac{y'}{R'}\right) \\
H_{R'} &= 0 \\
H_{\varphi'} &= ik \left(\frac{IL}{4\pi}\right) \left(\frac{e^{ikR'}}{R'}\right) \cos\vartheta' \cos\varphi' \\
H_{\vartheta'} &= ik \left(\frac{IL}{4\pi}\right) \left(\frac{e^{ikR'}}{R'}\right) \sin\varphi' \\
E_{\vartheta'} &= \eta_0 H_{\varphi'} \quad (TM,\ m = 1\ polarization) \\
E_{\varphi'} &= \eta_0 \quad (TE,\ m = 2\ polarization)
\end{aligned} \tag{1}$$

Pure TM or TE incident polarization will only occur in certain

directions. For example, $\phi = \frac{\pi}{2}$ corresponds to pure incident TE polarization.

From Figure 1:

$$\underline{e}_R = -\underline{e}_{R'}$$

or

$$\begin{aligned}
&\underline{e}_x \sin\vartheta_i(t)\cos\varphi_i(t) + \underline{e}_y \sin\vartheta_i(t)\sin\varphi_i(t) + \underline{e}_z \cos\vartheta_i(t) \\
&\quad = -\left[\underline{e}_{x'} \sin\vartheta'(t)\cos\varphi'(t) + \underline{e}_{y'} \sin\vartheta'(t)\sin\varphi'(t) + \underline{e}_{z'} \cos\vartheta'(t)\right] \\
&\quad = -\underline{e}_x \sin\vartheta'(t)\cos\varphi'(t) + \underline{e}_y \sin\vartheta'(t)\sin\varphi'(t) + \underline{e}_z \cos\vartheta'(t)
\end{aligned}$$

or

$$\vartheta_i(t) = \vartheta'(t)$$

and

$$\varphi_i(t) = \pi - \varphi'(t) \tag{2}$$

3. Antenna Platform Motion

From the motion of the observer in Figure 1,

$$\begin{aligned}
\underline{R}(t) &= \underline{R}_0 + \underline{v}(t - t_0) \\
&\quad \underline{e}_x x_0 + \underline{e}_y y_0 + \underline{e}_z z_0 + \underline{e}_x v_x (t - t_0)
\end{aligned} \tag{3}$$

and

$$\begin{aligned}
\cos\vartheta_i(t) &= \frac{-z_0}{R(t)} \\
\tan\varphi_i(t) &= \frac{y_0}{x_0 + v_x(t - t_0)}
\end{aligned}$$

and the incident vector spectra (Kern, 1981) in region 1 is

$$\begin{bmatrix} b_1(1,\underline{K}) \\ b_1(2,\underline{K}) \end{bmatrix} = \begin{bmatrix} \cos\vartheta_i(t)\cos\varphi_i(t) \\ \sin\varphi_i(t) \end{bmatrix}, \tag{4}$$

The vector spectra (column vector with second argument the wave number, $\underline{K}$) in Equation (4) is perpendicular to the incident propagation direction. The first argument in the parenthesis corresponds to either incident TM (first argument = 1) or TE (first argument = 2) polarization.

Although the motion of the radar platform is included in the above definitions, the numerical results which are presented later pertain to a fixed platform at some specified azimuth and elevation and range. The mathematics to include motion are presented for completeness.

4. Transmitted Fields in Medium 2

The direction of the incident field in medium 2 is determined from Snell's law,

$$\begin{aligned} \sin\theta &= \frac{\sin\vartheta_i(t)}{\sqrt{\epsilon'}} \\ \epsilon' &= \epsilon_r + \frac{i\sigma}{\omega\epsilon_0} \end{aligned} \tag{5}$$

and because the plane of incidence extends below the interface in both media,

$$\varphi = \varphi_i(t)$$

The electric field incident of the target in medium 2 is, using Kern's (1981) spectral representation

$$\begin{aligned} \underline{E}_2^{inc}\left(\underline{R}^i\right) &= \frac{\underline{a}_2(m,\underline{K})}{2\pi} e^{i\underline{k}\cdot\underline{R}^i} \\ \underline{a}_2(m,\underline{K}) &= a_2(1,\underline{K})\frac{\underline{e}_\vartheta}{\cos\vartheta} + a_2(2,\underline{K})\underline{e}_\varphi \end{aligned} \tag{6}$$

where the incident vector spectra in medium 2 is

$$\begin{bmatrix} a_2(1,\underline{K}) \\ a_2(2,\underline{K}) \end{bmatrix} = \begin{bmatrix} T_{21}(1)e^{ikd\cos\vartheta} & 0 \\ 0 & T_{21}(2)e^{ikd\cos\vartheta} \end{bmatrix} \begin{bmatrix} b_1(1,\underline{K}) \\ b_1(2,\underline{K}) \end{bmatrix} \tag{7}$$

and the transmission coefficients for TM and TE polarizations are

$$\begin{aligned} T_{21}(1) &= \frac{2\sqrt{\epsilon' - \sin^2\vartheta_i(t)}}{\sqrt{\epsilon' - \sin^2\vartheta_i(t)} + \epsilon'\cos\vartheta_i(t)} \\ T_{21}(2) &= \frac{2\cos\vartheta_i(t)}{\cos\vartheta_i(t) + \sqrt{\epsilon' - \sin^2\vartheta_i(t)}} \\ k &= k_0\sqrt{\epsilon'} \end{aligned} \tag{8}$$

$$\cos\theta = \frac{\sqrt{\epsilon' - \sin^2\vartheta_i}}{\sqrt{\epsilon'}} \tag{9}$$

The incident wave vector is

$$\underline{k} = k\left(\underline{e}_x\sin\vartheta\cos\varphi + \underline{e}_y\sin\vartheta\sin\varphi + \underline{e}_z\cos\vartheta\right) \tag{10}$$

In Equation (6) the unit vector $\underline{e}_\vartheta$ is divided by the $\cos\vartheta$ in Kern's definition of a vector "transverse" to the z-axis in Figure 1 in order that this transverse vector, $\underline{T}$ satisfy the two following conditions:

$$\begin{aligned} \underline{e}_k \cdot \underline{T} &= 0 \\ \underline{e}_p \cdot \underline{T} &= 1\ , \end{aligned} \tag{11}$$

where the transverse vector, $\underline{T}$ is in the plane of $\underline{e}_k$ and $\underline{e}_z$ and is given by

$$\underline{T} = \frac{\underline{e}_\vartheta}{\cos\vartheta} = \frac{\underline{e}_z}{\cos\vartheta\sin\vartheta} - \frac{\underline{e}_k}{\sin\vartheta} \tag{12}$$

which makes the component of $\underline{T}$ transverse to the z-axis have unity magnitude for all incident angles, ϑ.

5. Scattered Field in Medium 2

The spectra for the field scattered by the target in medium 2 is given in terms of the scattering matrix as

$$\begin{bmatrix} b_2(1,\underline{K}) \\ b_2(2,\underline{K}) \end{bmatrix} = \begin{bmatrix} S_{11} & S_{12} \\ S_{21} & S_{22} \end{bmatrix} \begin{bmatrix} a_2(1,\underline{K}) \\ a_2(2,\underline{K}) \end{bmatrix} \tag{13}$$

The derivation of the elements in the scattering matrix, uses the relation between the incident spectra in medium 2 and the asymptotic scattered far field in medium 2. The scattered field in medium 2 is given in terms of the induced dipole moment (electric and magnetic) on the scatterer as

$$\begin{aligned} \underline{p} &= \underline{\underline{\alpha}} \cdot \underline{E}_2^i \\ &\left(\underline{\underline{\alpha}}_e + \underline{\underline{\alpha}}_m\right) \cdot \underline{E}_2^i \end{aligned}$$

$$\begin{aligned} \underline{E}_2^s &= \frac{-k^2}{4\pi\epsilon} \left[\underline{e}_R \times (\underline{e}_R \times \underline{p})\right] \frac{e^{ikR}}{R} \\ &= -ik \cos\vartheta \underline{b}_2(m,\underline{K}) \frac{e^{ikR}}{R} \end{aligned} \tag{14}$$

$$\underline{\underline{\alpha}} = \begin{bmatrix} \alpha_{xx} & 0 & 0 \\ 0 & \alpha_{yy} & 0 \\ 0 & 0 & \alpha_{zz} \end{bmatrix}$$

where the components of the polarizability are given by (Van de Hulst, 1957, Ishimaru, 1991)

$$
\begin{aligned}
\alpha_{ii} &= \frac{V\epsilon_0}{L_i + \frac{1}{n^2-1}} \\
V &= \frac{4}{3}\pi abc = \frac{4}{3}\pi ca^2 \\
e^2 &= 1 - \left(\frac{a}{c}\right)^2 \\
L_z &= \frac{1-e^2}{e^2}\left(-1 + \frac{1}{2e}\ln\frac{1+e}{1-e}\right) \\
L_x &= L_Y = \frac{1}{2}(1 - L_z) \\
n^2 &= \epsilon_{r,\text{targ}} + \frac{i\sigma_{\text{targ}}}{\omega\epsilon_0}
\end{aligned}
\tag{15}
$$

where, for a prolate spheroid,

$$L_x = L_y < L_z \tag{16}$$

A prolate spheroid can be deformed into long needle-like objects (high Q scatterers) or a sphere (low Q scatterer). For a perfect conductor,

$$\alpha_i = \frac{V}{L_i}$$

Expanding the dipole moment,

$$
\begin{aligned}
\underline{p} &= (\alpha_{xx}\underline{e}_x\underline{e}_x + \alpha_{yy}\underline{e}_y\underline{e}_y + \alpha_{zz}\underline{e}_z\underline{e}_z) \\
&\quad \cdot \left[a_2(1,\underline{K})\frac{\underline{e}_\vartheta}{\cos} + a_2(2,\underline{K})\underline{e}_\varphi\right] \\
&= (\alpha_{xx}\underline{e}_x\underline{e}_x + \alpha_{yy}\underline{e}_y\underline{e}_y + \alpha_{zz}\underline{e}_z\underline{e}_z)\cdot \\
&\quad \cdot \left[\frac{a_2(1,\underline{K})}{\cos\vartheta}\left(\underline{e}_x\cos\vartheta\cos\varphi + \underline{e}_y\cos\vartheta\sin\varphi - \underline{e}_z\sin\vartheta\right)\right. \\
&\qquad \left. + a_2(2,\underline{K})\left(-\underline{e}_x\sin\varphi + \underline{e}_y\cos\varphi\right)\right] \qquad (17) \\
&= \alpha_{xx}\underline{e}_x\left[a_2(1,\underline{K})\cos\varphi - a_2(2,\underline{K})\sin\varphi\right] \\
&\quad + \alpha_{yy}\underline{e}_y[a_2(1,\underline{K})\sin\varphi + a_2(2,\underline{K})\cos\varphi] \\
&\quad - \alpha_{zz}\underline{e}_z a_2(1,\underline{K})\tan\vartheta \qquad (18)
\end{aligned}
$$

The components of the expansion of the vector triple product for the scattered electric field become

$$\begin{aligned}\underline{e}_R \cdot \underline{p} = {} & \alpha_{xx}\left[a_2(1,\underline{K})\sin\vartheta\cos^2\varphi - a_2(2,\underline{K})\sin\vartheta\sin\varphi\cos\varphi\right] \\ & + \alpha_{yy}\left[a_2(1,\underline{K})\sin\vartheta\sin^2\varphi + a_2(2,\underline{K})\sin\vartheta\sin\varphi\cos\varphi\right] \\ & - \alpha_{zz}a_2(1,\underline{K})\sin\vartheta\end{aligned} \tag{19}$$

$$\begin{aligned}&\underline{e}_R\left(\underline{e}_R\cdot\underline{p}\right) - \underline{p} = \\ &\underline{e}_x\left\{\begin{array}{c}\alpha_{xx}\left(\sin^2\vartheta\cos^2\varphi - 1\right)\left[a_2(1,\underline{K})\cos\varphi - a_2(2,\underline{K})\sin\varphi\right] \\ +\alpha_{yy}\sin^2\vartheta\sin\varphi\cos\varphi[a_2(1,\underline{K})\sin\varphi + a_2(2,\underline{K})\cos\varphi] \\ -\alpha_{zz}a_2(1,\underline{K})\sin^2\vartheta\cos\varphi\end{array}\right\} \\ &+\underline{e}_y\left\{\begin{array}{c}\alpha_{xx}\sin^2\vartheta\sin\varphi\cos\varphi[a_2(1,\underline{K})\cos\varphi - a_2(2,\underline{K})\sin\varphi] \\ +\alpha_{yy}(\sin^2\vartheta\sin^2\varphi - 1)[a_2(1,\underline{K})\sin\varphi + a_2(2,\underline{K})\cos\varphi] \\ -\alpha_{zz}a_2(1,\underline{K})\sin^2\vartheta\sin\varphi\end{array}\right\} \\ &+\underline{e}_z\left\{\begin{array}{c}\alpha_{xx}\sin\vartheta\cos\vartheta\cos\varphi[a_2(1,\underline{K})\cos\varphi - a_2(2,\underline{K})\sin\varphi] \\ +\alpha_{yy}\sin\vartheta\cos\vartheta\sin\varphi[a_2(1,\underline{K})\sin\varphi + a_2(2,\underline{K})\cos\varphi] \\ \alpha_{zz}a_2(1,\underline{K})\frac{\sin^3\vartheta}{\cos\vartheta}\end{array}\right\}\end{aligned} \tag{20}$$

Using Kern's expression for the vector spectrum for an elementary electric dipole of moment $\underline{p}$, from Example 2.2 - 4 on page 127,

$$\underline{b}_2(m,\underline{K}) = \left(\frac{-ik}{4\pi\epsilon_0\epsilon'}\right)\frac{\left[\underline{e}_R(\underline{e}_R\cdot\underline{p}) - \underline{p}\right]}{\cos\vartheta} \tag{21}$$

and the following alternate general expression for the vector scattered spectra in region 22 in terms of the scalar spectra,

$$\underline{b}_2(m,\underline{K}) = -\frac{b_2(1,\underline{K})}{\cos\vartheta}\underline{e}_\vartheta + b_2(2,\underline{K})\underline{e}_\varphi \tag{22}$$

which can be expanded in terms of its x-, y-, and x-components as

$$
\begin{aligned}
\underline{b}_2(m,\underline{K}) = & \\
& -\frac{b_2(1,\underline{K})}{\cos\vartheta}\left(\underline{e}_x\cos\vartheta\cos\varphi+\underline{e}_y\cos\vartheta\sin\varphi-\underline{e}_z\sin\vartheta\right) \\
& +b_2(2,\underline{K})(-\underline{e}_x\sin\varphi+\underline{e}_y\cos\varphi) \\
& =-\underline{e}_x(b_2(1,\underline{K})\cos\varphi+b_2(2,\underline{K})\sin\varphi) \\
& \quad +\underline{e}_y(-b_2(1,\underline{K})\sin\varphi+b_2(2,\underline{K})\cos\varphi) \\
& \quad +\underline{e}_z b_2(1,\underline{K})\frac{\sin\vartheta}{\cos\vartheta}
\end{aligned}
\tag{23}
$$

and equating Equations (21) and (43) (except for the term $\frac{-ik}{4\pi\epsilon}$) yields the components of the scattered in terms of the polarizability of the scatterer

$$
\begin{aligned}
b_2(1,\underline{K}) = & \alpha_{xx}\cos\vartheta\cos\phi[a_2(1,\underline{K})\cos\varphi-a(2,\underline{K})\sin\varphi] \\
& +\alpha_{yy}\cos\vartheta\sin\varphi[a_2(1,\underline{K})\sin\varphi+a_2(2,\underline{K})\cos\varphi] \\
& +\alpha_{zz}a_2(2,\underline{K})\frac{\sin^2\vartheta}{\cos\vartheta}
\end{aligned}
\tag{24}
$$

$$
\begin{aligned}
b_2(2,\underline{K}) = & \alpha_{xx}\left(\frac{\sin\varphi}{\cos\vartheta}\right)[a_2(1,\underline{K})\cos\varphi-a_2(2,\underline{K})\sin\varphi] \\
& -\alpha_{yy}\left(\frac{\cos\varphi}{\cos\vartheta}\right)[a_2(1,\underline{K})\sin\varphi+a_2(2,\underline{K})\cos\varphi]
\end{aligned}
$$

The scattering matrix in medium 2 becomes

$$
\begin{bmatrix} S_{11} & S_{12} \\ S_{21} & S_{22} \end{bmatrix} =
$$

$$
\begin{bmatrix}
\left[\cos\vartheta(\alpha_{xx}\cos^2\varphi+\alpha_{yy}\sin^2\varphi)+\alpha_{zz}\frac{\sin^2\vartheta}{\cos\vartheta}\right] & -\frac{\sin\varphi\cos\varphi}{\cos\vartheta}(\alpha_{xx}-\alpha_{yy}) \\
\cos\vartheta\sin\varphi\cos\varphi(\alpha_{xx}-\alpha_{yy}) & -\frac{1}{\cos\vartheta}(\alpha_{xx}\sin^2\varphi+\alpha_{yy}\cos^2\varphi)
\end{bmatrix}
\tag{25}
$$

Neglecting multiple reflections between the target and the interface, the scattered spectra in region 1 becomes the sum of the specular reflection from the interface (if the surface is rough this term is modified by an additional rough surface scattering matrix as will be shown later) and the return from the buried object as

$$\begin{bmatrix} a_1(1,\underline{K}) \\ a_1(2,\underline{K}) \end{bmatrix} = \begin{bmatrix} R_{11}(1) & 0 \\ 0 & R_{11}(2) \end{bmatrix} \begin{bmatrix} b_1(1,\underline{K}) \\ b_1(2,\underline{K}) \end{bmatrix} + \begin{bmatrix} T_{12}(1)e^{ikd\cos\vartheta} & 0 \\ 0 & T_{12}(2)e^{ikd\cos\vartheta} \end{bmatrix} \begin{bmatrix} b_2(1,\underline{K}) \\ b_2(2,\underline{K}) \end{bmatrix}$$

$$\begin{aligned} T_{12}(1) &= \frac{2\epsilon'\cos\vartheta_i(t)}{\epsilon'\cos\vartheta_i(t) + \sqrt{\epsilon' - \sin^2\vartheta_i(t)}} \\ T_{12}(2) &= \frac{2\sqrt{\epsilon' - \sin^2\vartheta_i(t)}}{\cos\vartheta_i(t) + \sqrt{\epsilon' - \sin^2\vartheta_i(t)}} \end{aligned} \tag{26}$$

$$\begin{aligned} R_{11}(1) &= \frac{-\epsilon'\cos\vartheta_i + \sqrt{\epsilon' - \sin^2\vartheta_i(t)}}{\epsilon'\cos\vartheta_i + \sqrt{\epsilon' - \sin^2\vartheta(t)}} \\ R_{11}(2) &= \frac{\cos\vartheta_i(t) - \sqrt{\epsilon' - \sin^2\vartheta(t)}}{\cos\vartheta_i(t) + \sqrt{\epsilon' - \sin^2\vartheta(t)}} \end{aligned}$$

In Equation (26), $R_{11}(1)$ is the negative of the usual difinition because of the direction of the positive axis in Figure 1, and θ is measured with respect to the negative z-axis. Note, that the effects of refraction in medium 2 are taken into account in the transmission matrix in Equation (26) in the argument of the exponentials where both the wave number, k, and the angle ϑ, the wave makes with the z-axis in medium 2. The transmission coefficients, $T_{12}(1)$, and $T_{12}(2)$ also include the refraction effects of medium 2.

6. Scattered Field in Medium 1

The scattered far-field in region 1 in terms of the scattered spectra is (derived by performing a stationary phase integration on $\int_{-\infty}^{\infty} dk_x \int_{\infty}^{\infty} dk_y f(\gamma, k_x, k_y)$)

$$\underline{E}_1^S = -ik_0|\cos\vartheta_i(t)|\frac{e^{ik_0R}}{R}\left[a_1(1,\underline{K})\frac{\underline{e}_\vartheta}{\cos\vartheta_i(t)} + a_1(2,\underline{K})\underline{e}_\varphi\right] \tag{27}$$

The factor $\cos\vartheta$ comes from the stationary phase integration as follows. The integral is given by

$$\int_{-\infty}^{\infty} dk_x \int_{-\infty}^{\infty} dk_y e^{i(k_x x + k_y y - z\sqrt{k^2-k_x^2-k_y^2})} f(k_x, k_y) \tag{28}$$

and the stationary phase points are solutions to

$$\begin{aligned} \left(\frac{\delta g}{\delta k_x}\right) &: x - \frac{z}{\sqrt{k^2-k_x^2-k_y^2}} = 0 \\ \left(\frac{\delta g}{\delta k_y}\right) &: y - \frac{z}{\sqrt{k^2-k_x^2-k_y^2}} = 0 \end{aligned} \tag{29}$$

$$g = k_x x + k_y y - z\sqrt{k^2-k_x^2-k_y^2}$$

and the amplitude term from the stationary phase integration gives

$$\frac{1}{\sqrt{\frac{\delta^2 g}{\delta k_x^2}\frac{\delta^2 g}{\delta k_y^2} - \left(\frac{\delta^2 g}{\delta k_x \delta k_y}\right)^2}} = k\cos\vartheta \tag{30}$$

Explicitly, the vector spectra in medium 1 in terms of the scattering matrix, the transmission and reflection coefficients and the propagation loss through the medium are

$$
\begin{aligned}
a_1(1,\underline{K}) &= R_{11}(1)\cos\vartheta_i(t)\cos\varphi_i(t) \\
&\quad + \left(\frac{k_0}{4\pi}\right) e^{i2k_0 d\sqrt{\epsilon' - sin^2\vartheta_i(t)}} \\
&\qquad \begin{bmatrix} T_{12}(1)S_{11}T_{21}(1)\cos\vartheta_i(t)\cos\varphi_i(t) \\ -T_{12}(1)S_{12}T_{21}(2)\sin\varphi_i(t) \end{bmatrix} \\
a_1(2,\underline{K}) &= R_{11}(2)\sin\varphi_i(t) \\
&\quad + \left(\frac{k_0}{4\pi}\right) e^{i2k_0 d\sqrt{\epsilon' - \sin^2\vartheta_i(t)}} \\
&\qquad \begin{bmatrix} T_{12}(2)S_{21}T_{21}(1)\cos\vartheta_i(t)\cos\varphi_i(t) \\ -T_{12}(2)S_{22}T_{21}(2)\sin\varphi_i(t) \end{bmatrix}
\end{aligned}
\tag{31}
$$

which includes the effects of refraction in medium 2 in the transmission coefficient terms in the matrices, and in the argument of the exponential multiplying the matrices. This refraction changes the wave direction, or scattering pattern of the buried target in going from medium 2 to medium 1. This is the same approach used by Hill (1988).

7. Multiple Reflections

When a single multiply reflected ray between the target and the interface occurs, the scattered spectra, in Equation (31) is modified, assuming plane wave scatter in medium 1, as

$$\begin{bmatrix} a_1(1,\underline{K}) \\ a_1(2,\underline{K}) \end{bmatrix} = \begin{bmatrix} R_{11}(1) & 0 \\ 0 & R_{11}(2) \end{bmatrix} \begin{bmatrix} b_1(1,\underline{K}) \\ b_1(2,\underline{K}) \end{bmatrix}$$
$$+ \begin{bmatrix} T_{12}(1)e^{ikd\cos\vartheta} & 0 \\ 0 & T_{12}(2)e^{ikd\cos\vartheta} \end{bmatrix} \begin{bmatrix} S_{11} & S_{12} \\ S_{21} & S_{22} \end{bmatrix} \cdot$$
$$\cdot \begin{bmatrix} T_{21}(1)e^{ikd\cos\vartheta} & 0 \\ 0 & T_{21}(2)e^{ikd\cos\vartheta} \end{bmatrix} \begin{bmatrix} b_1(1,\underline{K}) \\ b_1(2,\underline{K}) \end{bmatrix}$$
$$+ \begin{bmatrix} T_{12}(1)e^{ikd\cos\vartheta} & 0 \\ 0 & T_{12}(2)e^{ikd\cos\vartheta} \end{bmatrix} \begin{bmatrix} S_{11} & S_{12} \\ S_{21} & S_{22} \end{bmatrix} \cdot \tag{32}$$
$$\cdot \begin{bmatrix} R_{22}(1)e^{i2kd\cos\vartheta} & 0 \\ 0 & R_{22}(2)e^{i2kd\cos\vartheta} \end{bmatrix}$$
$$\cdot \begin{bmatrix} S_{11} & S_{12} \\ S_{21} & S_{22} \end{bmatrix} \begin{bmatrix} T_{21}(1)e^{ikd\cos\vartheta} & 0 \\ 0 & T_{21}(2)e^{ikd\cos\vartheta} \end{bmatrix} \cdot$$
$$\cdot \begin{bmatrix} b_1(1,\underline{K}) \\ b_1(2,\underline{K}) \end{bmatrix}$$

and performing the multiplication's in the last three matrices in Equation (32) gives the following intermediate result

$$\begin{bmatrix} T_{21}(1)S_{11}e^{ikd\cos\vartheta}b_1(1,\underline{K}) & T_{21}(2)S_{12}e^{ikd\cos\vartheta}b_1(2,\underline{K}) \\ T_{21}(1)S_{21}e^{ikd\cos\vartheta}b_1(1,\underline{K}) & T_{21}(2)S_{22}e^{ikd\cos\vartheta}b_1(2,\underline{K}) \end{bmatrix} \tag{33}$$

and multiplying (33) by the last matrix on line 3 of Equation (32) gives the next intermediate result

$$\begin{bmatrix} R_{22}(1)T_{21}(1)S_{11}e^{i3kd\cos\vartheta}b_1(1,\underline{K}) \\ R_{22}(2)T_{21}(1)S_{21}e^{i3kd\cos\vartheta}b_1(1,\underline{K}) \\ R_{22}(1)T_{21}(2)S_{12}e^{i3kd\cos\vartheta}b_1(2,\underline{K}) \\ R_{22}(2)T_{21}(2)S_{22}e^{i3kd\cos\vartheta}b_1(2,\underline{K}) \end{bmatrix} \tag{34}$$

and multiplying (34) by the second matrix on line 3 of Equation (32) gives the next intermediate result

$$\begin{bmatrix} \begin{pmatrix} R_{22}(1)T_{21}(1)S_{11}^2 e^{i3kd\cos\vartheta} b_1(1,\underline{K}) \\ +R_{22}(2)T_{21}(1)S_{21}S_{12}e^{i3kd\cos\vartheta} b_1(1,\underline{K}) \end{pmatrix} & \begin{pmatrix} R_{22}(1)T_{21}(2)S_{12}S_{11}e^{i3kd\cos\vartheta} b_1(2,\underline{K}) \\ +R_{22}(2)T_{21}(2)S_{12}S_{22}e^{i3kd\cos\vartheta} b_1(2,\underline{K}) \end{pmatrix} \\ \begin{pmatrix} R_{22}(1)T_{21}(1)S_{11}S_{21}e^{i3kd\cos\vartheta} b_1(1,\underline{K}) \\ +R_{22}(2)T_{21}(1)S_{21}S_{22}e^{i3kd\cos\vartheta} b_1(1,\underline{K}) \end{pmatrix} & \begin{pmatrix} R_{22}(1)T_{21}(2)S_{12}S_{21}e^{i3kd\cos\vartheta} b_1(2,\underline{K}) \\ +R_{22}(2)T_{21}(2)S_{22}^2 e^{i3kd\cos\vartheta} b_1(2,\underline{K}) \end{pmatrix} \end{bmatrix} \tag{35}$$

and multiplying (35) by the first matrix on line 3 of Equation (32) gives the next intermediate result

$$\begin{bmatrix} \begin{pmatrix} R_{22}(1)T_{21}(1)T_{12}(1)S_{11}^2 e^{i4kd\cos\vartheta} b_1(1,\underline{K}) \\ +R_{22}(2)T_{21}(1)T_{12}(1)S_{21}S_{12}e^{i4kd\cos\vartheta} b_1(1,\underline{K}) \end{pmatrix} & \begin{pmatrix} R_{22}(1)T_{21}(2)T_{12}(1)S_{12}S_{11}e^{i4kd\cos\vartheta} b_1(2,\underline{K}) \\ +R_{22}(2)T_{21}(2)T_{12}(1)S_{12}S_{22}e^{i4kd\cos\vartheta} b_1(2,\underline{K}) \end{pmatrix} \\ \begin{pmatrix} R_{22}(1)T_{21}(1)T_{12}(2)S_{11}S_{21}e^{i4kd\cos\vartheta} b_1(1,\underline{K}) \\ +R_{22}(2)T_{21}(1)T_{12}(2)S_{21}S_{22}e^{i4kd\cos\vartheta} b_1(1,\underline{K}) \end{pmatrix} & \begin{pmatrix} R_{22}(1)T_{21}(2)T_{12}(2)S_{12}S_{21}e^{i4kd\cos\vartheta} b_1(2,\underline{K}) \\ +R_{22}(2)T_{21}(2)T_{12}(2)S_{22}^2 e^{i4kd\cos\vartheta} b_1(2,\underline{K}) \end{pmatrix} \end{bmatrix} \tag{36}$$

which can be factored to yield the final result for the spectra in region 1, for the multiple bounce as

$$\begin{aligned} a_1(1,\underline{K}) &= \left(\frac{k_0}{4\pi}\right) T_{12}(1) e^{i4kd\cos\vartheta} \\ &\quad \left\{ \begin{array}{l} [R_{22}(1)S_{11}^2 + R_{22}(2)S_{21}S_{12}]T_{21}(1)b_1(1,\underline{K}) \\ +[R_{22}(1)S_{11} + R_{22}(2)S_{22}]T_{21}(2)S_{12}b_1(2,\underline{K}) \end{array} \right\} \\ a_1(2,\underline{K}) &= \left(\frac{k_0}{4\pi}\right) T_{12}(2) e^{i4kd\cos\vartheta} \\ &\quad \left\{ \begin{array}{l} [R_{22}(1)S_{11} + R_{22}(2)S_{22}]T_{21}(1)S_{21}b_1(1,\underline{K}) \\ +[R_{22}(1)S_{12}S_{21} + R_{22}(2)S_{22}^2]T_{21}(2)b_1(2,\underline{K}) \end{array} \right\} \end{aligned} \tag{37}$$

Equation (37) can be substituted into Equation (27) to find the scattered field in region 1. In addition, the multiple bounce requires the following two additional reflection coefficients

$$\begin{aligned} R_{22}(1) &= \frac{\epsilon'\cos\vartheta_i(t) - \sqrt{\epsilon' - \sin^2\vartheta_i(t)}}{\epsilon'\cos\vartheta_i(t) + \sqrt{\epsilon' - \sin^2\vartheta_i(t)}} \\ R_{22}(2) &= \frac{-\cos\vartheta_i(t) + \sqrt{\epsilon' - \sin^2\vartheta_i(t)}}{\cos\vartheta_i(t) + \sqrt{\epsilon' - \sin^2\vartheta_i(t)}} \end{aligned} \tag{38}$$

8. Diffuse Scatter from a 2-D Facet Interface

Although the main EM rough surface back scatter result is for the case of a 3-D interface in the next section, the 2-D case is also included for completeness. When the interface between the two media is rough the scattered spectra in region 1 need to be multiplied by an additional scattering matrix representing the rough surface as

$$\begin{bmatrix} R_{11}(1) & 0 \\ 0 & R_{11}(2) \end{bmatrix} \begin{bmatrix} b_1(1,\underline{K}) \\ b_1(2,\underline{K}) \end{bmatrix} \begin{bmatrix} S_{11}^{rough}(1) & 0 \\ 0 & S_{11}^{rough}(2) \end{bmatrix} \tag{39}$$

where the "roughness scattering matrix" is derived using the following rigorous expression for the field scattered by the terrain in terms of the surface currents

$$\underline{E}^S(\underline{r}) = ik\eta_0 \int_{L_i} \underline{\underline{\Gamma}} \cdot \underline{J} dl + \int_{L_i} \underline{\nabla} G \times \underline{K} dl, \tag{40}$$

with the geometry for the faceted surface shown in Figure 2 together with the geometry for the scattered field in Equation (40).

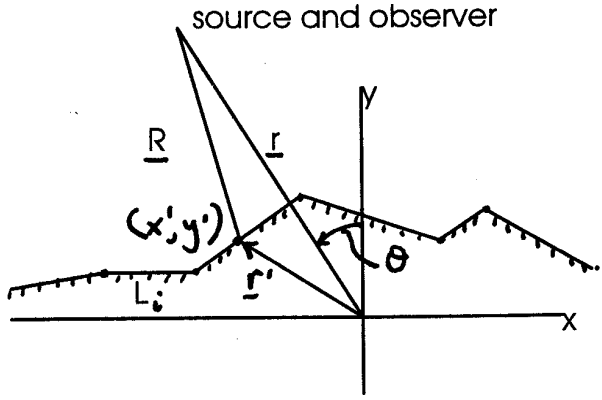

Figure 2. Geometry for 2-D scatter from a faceted surface.

In Equation (40) the dyadic Green's function is

$$\underline{\underline{\Gamma}} = \left(\underline{\underline{I}} + \frac{1}{k^2} \underline{\nabla}' \underline{\nabla}' \right) G \tag{41}$$

and

$$\begin{aligned} \underline{\nabla}' G &\cong -ik \underline{e}_R G \\ &\cong -ik \left(-\underline{e}_x \sin\theta_i(t) + \underline{e}_y \cos\theta_i(t) \right) G \end{aligned} \tag{42}$$

so that

$$\underline{\underline{\Gamma}} = \begin{bmatrix} \underline{e}_x \underline{e}_x \cos^2\theta_i(t) & \underline{e}_x \underline{e}_y \sin\theta_i(t) \cos\theta_i(t) & 0 \\ \underline{e}_y \underline{e}_x \sin\theta_i(t) \cos\theta_i(t) & \underline{e}_y \underline{e}_y \sin^2\theta_i(t) & 0 \\ 0 & 0 & \underline{e}_z \underline{e}_z \end{bmatrix} \tag{43}$$

The electric and magnetic currents in Equation (40) are

$$\begin{aligned} \underline{J} &= \underline{J}_{TE} + \underline{J}_{TM} \\ \underline{K} &= \underline{K}_{TE} + \underline{K}_{TM} \end{aligned} \tag{44}$$

and in terms of the incident field are given by

$$\begin{aligned} \underline{J}_{TE} &= (1 - R_{TE}) \left(\underline{H}^{inc} \cdot \underline{e}_T \right) \underline{e}_z \\ \underline{J}_{TM} &= -(1 + R_{TM}) \left(\underline{H}^{inc} \cdot \underline{e}_z \right) \underline{e}_T \\ \underline{K}_{TE} &= (1 + R_{TE}) \left(\underline{E}^{inc} \cdot \underline{e}_z \right) \underline{e}_T \\ \underline{K}_{TM} &= -(1 - R_{TM}) \left(\underline{E}^{inc} \cdot \underline{e}_T \right) \underline{e}_z \end{aligned} \tag{45}$$

and the unit-normal and unit-tangent vectors are given by

$$\begin{aligned} \underline{e}_n &= \frac{-y'(x)\underline{e}_x + \underline{e}_y}{\sqrt{a + (y')^2}} \\ \underline{e}_T &= \frac{-y'(x)\underline{e}_y + \underline{e}_x}{\sqrt{1 + (y')^2}} = \underline{e}_z \times \underline{e}_n \end{aligned} \tag{46}$$

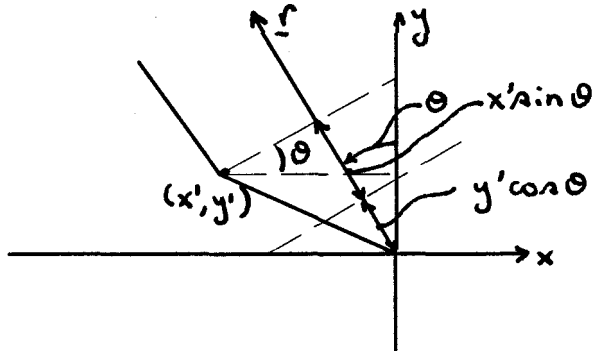

Figure 3. Geometry for approximating the distance R in the far-field.

If the source and observer are in the far-field, the distance R can be approximated as follows together with the help of Figure 3.

$$\begin{aligned} R &= \sqrt{(x-x')^2+(y-y')^2} \\ &\cong \sqrt{x^2-2xx'+y^2-2yy'} \\ &\cong \sqrt{r^2-2(xx'+yy')} \\ &\cong r-\left(x'\sin\theta_i(t)+y'\cos\theta_i(t)\right) \end{aligned} \tag{47}$$

The incident fields for the TM case is

$$\begin{aligned} \underline{E}^{inc} &= \left(\underline{e}_x\cos\vartheta_i(t)+\underline{e}_y\sin\theta_i(t)\right)e^{-ik(x'\sin\theta_i(t)+y'\cos\theta_i(t))} \\ \underline{H}^{inc} &= \frac{\underline{e}_z}{\eta_0}e^{-ik(x'\sin\theta_i(t)+y'\cos\theta_i(t))} \end{aligned} \tag{48}$$

and for the TE case

$$\begin{aligned} \underline{E}^{inc} &= \underline{e}_z e^{-ik(x'\sin\theta_i(t)+y'\cos\theta_i(t))} \\ \underline{H}^{inc} &= \frac{-1}{\eta_0}\left(\underline{e}_x\cos\theta_i(t)+\underline{e}_y\sin\theta_i(t)\right)e^{-ik(x'\sin\theta_i(t)+y'\cos\theta_i(t))} \end{aligned} \tag{49}$$

The elemental integration length dl is

$$dl = \sqrt{1+[y'(x)]^2}dx' \tag{50}$$

and substituting Equations (42) through (50) into Equation (40) yields the following scattered field for TM polarization

$$\underline{E}^S_{TM} = -\underline{e}_\varphi 2ikR_{TM}\frac{e^{ikr}}{r}I_i \tag{51}$$

where the integration over the i-th segment is given by

$$I_i = \int_{x_i}^{x_{i+t}}\left(\cos\vartheta_i - \frac{dh}{dx'}\sin\vartheta_i\right)e^{-i2k(x'\sin\theta_i(t)+h(x')\cos\theta_i(t))}dx' \tag{52}$$

and h(x) is the height of the terrain. Similarly, the scattered TE field is

$$\underline{E}^S_{TE} = -2ikR_{TE}\underline{e}_z \frac{e^{ikr}}{r} I_i \tag{53}$$

The total scattered field for the TM and TE cases is obtained by summing over the total number of segments. This result assumes the segment lengths are longer than the wavelength and that almost no shadowing occurs.

9. Diffuse Scatter from a 3-D Facet Interface

The geometry for the 3-D problem is shown in Figure 4.

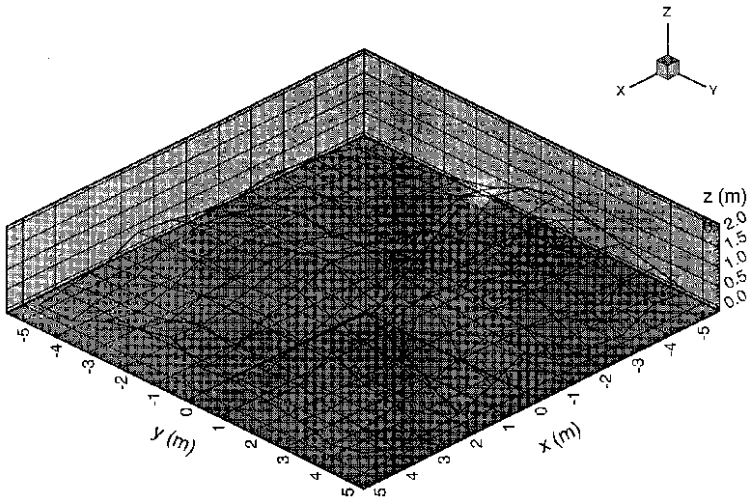

Figure 4. Geometry for the coherent backscatter from a 3-D rough surface.

The scattered field in terms of the surface currents is (Chew, 1995, p.32, eq'n. 1.4.20), in analogy with Equation (40), for $e^{-i\omega t}$ time convention,

$$\underline{E}^s(\underline{r}) = -\int_{x_1}^{x_2} dx' \int_{y_1}^{y_2} dy' \left(-i\omega\mu_0 \underline{\underline{\Gamma}} \cdot \underline{J} + \underline{K} \times \underline{\nabla} G\right) (\underline{e}_z \cdot \underline{e}_n)^{-1} \tag{54}$$

and since $\underline{J} \propto \frac{1}{\eta_0}$ and $\underline{\nabla} G = -\underline{\nabla}' G$,

$$\underline{E}^s(\underline{r}) = \int_{x_1}^{x_2} dx' \int_{y_1}^{y_2} dy' \left(ik \underline{\underline{\Gamma}} \cdot \underline{J} + \underline{K} \times \underline{\nabla}' G \right) (\underline{e}_z \cdot \underline{e}_n)^{-1} \tag{55}$$

In Equation (55), the terms in the integrand are

$$\begin{aligned} \underline{\underline{\Gamma}} &= \left(\underline{\underline{I}} + \frac{1}{k^2} \underline{\nabla}' \underline{\nabla}' \right) G\left(\underline{r}, \underline{r}'\right) \\ G\left(\underline{r}, \underline{r}'\right) &= \frac{e^{ikR}}{4\pi R}, \quad R = \sqrt{(x-x')^2 + (y-y')^2 + (z-z')^2} \\ \underline{\nabla}' G &\cong -ik \underline{e}_R G \end{aligned} \tag{56}$$

In the Fraunhoffer region, and for the backscatter case,

$$\begin{aligned} \underline{e}_R &\cong \underline{e}_r = \underline{e}_x \sin\vartheta_i \cos\varphi_i + \underline{e}_y \sin\vartheta_i \sin\varphi_i + \underline{e}_z \cos\vartheta_i \\ \underline{\nabla}' \underline{\nabla}' &= -k^2 \underline{e}_R \underline{e}_R G \end{aligned} \tag{57}$$

and substituting (57) into (56)

$$\underline{\underline{\Gamma}} = \left[\begin{array}{ccc} \underline{e}_x \underline{e}_x (1 - \sin^2\vartheta_i \cos^2\varphi_i) & -\underline{e}_x \underline{e}_y \sin^2\vartheta_i \sin\varphi_i \cos\varphi_i & -\underline{e}_x \underline{e}_z \sin\vartheta_i \cos\vartheta_i \cos\varphi_i \\ -\underline{e}_y \underline{e}_x \sin^2\vartheta_i \sin\varphi_i \cos\varphi_i & \underline{e}_y \underline{e}_y \left(1 - \sin^2\theta_i \sin^2\varphi_i\right) & -\underline{e}_y \underline{e}_z \sin\vartheta_i \cos\vartheta_i \sin\varphi_i \\ -\underline{e}_z \underline{e}_x \sin\vartheta_i \cos\vartheta_i \cos\varphi_i & -\underline{e}_y \underline{e}_y \sin\vartheta_i \cos\vartheta_i \sin\varphi_i & \underline{e}_z \underline{e}_z \sin^2\vartheta_i \end{array} \right] \left(\frac{e^{ikR}}{4\pi R} \right) \tag{58}$$

The incident TM and TE electric fields are

$$\begin{aligned} \underline{E}^{inc}_{TE} &= \left(\underline{E}^{inc} \cdot \underline{e}_T\right) \underline{e}_T \\ \underline{E}^{inc}_{TM} &= \underline{E}^{inc} - \left(\underline{E}^{inc} \cdot \underline{e}_T\right) - \left(\underline{E}^{inc} \cdot \underline{e}_n\right) \underline{e}_n \\ \underline{e}_T &= \frac{\underline{e}_R \times \underline{e}_n}{|\underline{e}_R \times \underline{e}_n|} = \left[\begin{array}{c} \underline{e}_x (\sin\vartheta_i \sin\varphi_i + \zeta_y \cos\vartheta_i) \\ +\underline{e}_y (-\sin\vartheta_i \cos\varphi_i - \zeta_x \cos\vartheta_i) \\ +\underline{e}_z (\zeta_x \sin\vartheta_i \sin\varphi_i - \zeta_y \sin\vartheta_i \cos\varphi_i) \end{array} \right] \end{aligned} \tag{59}$$

where only terms to the first order in the slope have been retained, and the total (incident plus reflected fields) on the rough surface are

$$
\begin{aligned}
\underline{E}_{TE}^{total} &= (1+R_{TE})\left(\underline{E}^{inc}\cdot\underline{e}_T\right)\underline{e}_T \\
\underline{E}_{TM}^{total} &= (1-R_{TM})\left[\underline{E}^{inc}-\left(\underline{E}^{inc}\cdot\underline{e}_T\right)\underline{e}_T-\left(\underline{E}^{inc}\cdot\underline{e}_n\right)\underline{e}_n\right] \\
\underline{H}_{TM}^{total} &= (1-R_{TM})\left(\underline{H}^{inc}\cdot\underline{e}_T\right)\underline{e}_T \\
\underline{H}_{TE}^{total} &= (1-R_{TE})\left[\underline{H}^{inc}-\left(\underline{H}^{inc}\cdot\underline{e}_T\right)\underline{e}_T-\left(\underline{H}^{inc}\cdot\underline{e}_n\right)\underline{e}_n\right] \\
\underline{E}^{total} &= \underline{E}_{TE}^{total}+\underline{E}_{TM}^{total} \\
&= (1-R_{TM})\,\underline{E}^{inc}+(R_{TE}+R_{TM})\left(\underline{E}^{inc}\cdot\underline{e}_T\right)\underline{e}_T \\
&\quad -(1-R_{TM})\left(\underline{E}^{inc}\cdot\underline{e}_n\right)\underline{e}_n \\
\underline{H}^{total} &= \underline{H}_{TE}^{total}+\underline{H}_{TM}^{total} \\
&= (1-R_{TE})\underline{H}^{inc}+(R_{TE}+R_{TM})\left(\underline{H}^{inc}\cdot\underline{e}_T\right)\underline{e}_T \\
&\quad -(1-R_{TE})\left(\underline{H}^{inc}\cdot\underline{e}_n\right)\underline{e}_n
\end{aligned}
\tag{60}
$$

Then, the total electric and magnetic currents on the surface are

$$
\begin{aligned}
\underline{K} &= -\underline{e}_n\times\underline{E}^{total} \\
&= -(1-R_{TM})\left(\underline{e}_n\times\underline{E}^{inc}\right) \\
&\quad -(R_{TE}+R_{TM})\left(\underline{E}^{inc}\cdot\underline{e}_T\right)\left[\underline{e}_R-\underline{e}_n(\underline{e}_R\cdot\underline{e}_n)\right] \\
\underline{J} &= \underline{e}_n\times\underline{H}^{total} \\
&= (1-R_{TE})\left(\underline{e}_n\times\underline{H}^{inc}\right) \\
&\quad +(R_{TE}+R_{TM})\left(\underline{H}^{inc}\cdot\underline{e}_T\right)\left[\underline{e}_R-\underline{e}_n(\underline{e}_R\cdot\underline{e}_n)\right]
\end{aligned}
\tag{61}
$$

For the case of a TM incident wave:

$$\begin{aligned}
\underline{E}^{inc} &= \underline{e}_{\vartheta} e^{-ikr} \\
&\quad \left(\underline{e}_x \cos\vartheta_i \cos\varphi_i + \underline{e}_y \cos\vartheta_i \sin\varphi_i - \underline{e}_z \sin\vartheta_i\right) \\
&\quad \cdots e^{-ik(x' \sin\vartheta_i \cos\varphi_i + y' \sin\vartheta_i \sin\varphi_i + z' \cos\vartheta_i)} \\
\underline{H}^{inc} &= \left(\frac{-\underline{e}_{\varphi}}{\eta_0}\right) e^{-ikr} \\
&\quad \frac{\left(\underline{e}_x \sin\varphi_i - \underline{e}_y \cos\varphi_i\right)}{\eta_0} \\
&\quad \cdots e^{-ik(x' \sin\vartheta_i \cos\varphi_i + y' \sin\vartheta_i \sin\varphi_i + z' \cos\vartheta_i)}
\end{aligned} \tag{62}$$

and for a TE incident wave

$$\begin{aligned}
\underline{E}^{inc} &= \underline{e}_{\varphi} e^{-ikr} \\
&= \frac{\left(-\underline{e}_x \sin\varphi_i + \underline{e}_y \cos\varphi_i\right)}{\eta_0} \\
&\quad \cdots e^{-ik(x' \sin\vartheta_i \cos\varphi_i + y' \sin\vartheta_i \sin\varphi_i + z' \cos\vartheta_i)} \\
\underline{H}^{inc} &= \frac{\underline{e}_{\vartheta}}{\eta_0} e^{-ikr} \\
&= \frac{\left(\underline{e}_x \cos\vartheta_i \cos\varphi_i + \underline{e}_y \cos\vartheta_i \sin\varphi_i - \underline{e}_z \sin\vartheta_i\right)}{\eta_0} \\
&\quad \cdots e^{-ik(x' \sin\vartheta_i \cos\varphi_i + y' \sin\vartheta_i \sin\varphi_i + z' \cos\vartheta_i)}
\end{aligned} \tag{63}$$

Performing the algebra for the TM case:

$$
\begin{aligned}
\underline{e}_n \times \underline{E}^{inc} &= \left[\begin{array}{c} \underline{e}_x\,(\zeta_y \sin\vartheta_i - \cos\vartheta_i \sin\varphi_i) + \\ \underline{e}_y\,(-\zeta_x \sin\vartheta_i + \cos\vartheta_i \cos\varphi_i) \\ +\underline{e}_z\,(-\zeta_x \cos\vartheta_i \sin\varphi_i + \zeta_y \cos\vartheta_i \cos\varphi_i) \end{array}\right] e^{-ikr} \\
\underline{E}^{inc} \cdot \underline{e}_T &= (-\zeta_x \sin\varphi_i + \zeta_y \cos\varphi_i)\ e^{-ikr} \\
\underline{e}_R - \underline{e}_n\,(\underline{e}_R \cdot \underline{e}_n) &= \underline{e}_x\,(\sin\vartheta_i \cos\varphi_i + \zeta_x \cos\vartheta_i) + \\
&\quad \cdots + \underline{e}_y\,(\sin\vartheta_i \sin\varphi_i + \zeta_y \cos\vartheta_i) + \\
&\quad \cdots + \underline{e}_z\,(\zeta_x \sin\vartheta_i \cos\varphi_i + \zeta_y \sin\vartheta_i \sin\varphi_i) \\
\left(\underline{E}^{inc} \cdot \underline{e}_T\right)\left[\underline{e}_R - \underline{e}_n\,(\underline{e}_R \cdot \underline{e}_n)\right] &= \\
&\left[\begin{array}{c} \underline{e}_x\,(-\zeta_x \sin\varphi_i + \zeta_y \cos\varphi_i) \\ (\sin\vartheta_i \cos\varphi_i + \zeta_x \cos\vartheta_i) \\ +\underline{e}_y\,(-\zeta_x \sin\varphi_i + \zeta_y \cos\varphi_i) \\ (\sin\vartheta_i \sin\varphi_i + \zeta_y \cos\vartheta_i) \\ +\underline{e}_z\,(-\zeta_x \sin\varphi_i + \zeta_y \cos\varphi_i) \\ (\zeta_x \sin\vartheta_i \cos\varphi_i + \zeta_y \sin\vartheta_i \sin\varphi_i) \end{array}\right]
\end{aligned}
\tag{64}
$$

and substituting (64) into (61) gives

$$
\underline{K} = -\left\{\begin{array}{c} (1 - R_{TM}) \\ \left[\begin{array}{c} \underline{e}_x(\zeta_y \sin\vartheta_i - \cos\vartheta_i \sin\varphi_i) \\ +\underline{e}_y(-\zeta_x \sin\vartheta_i + \cos\vartheta_i \cos\varphi_i) \\ +\underline{e}_z(-\zeta_x \cos\vartheta_i \sin\varphi_i + \zeta_y \cos\vartheta_i \cos\varphi_i) \end{array}\right] \\ (R_{TE} + R_{TM})(-\zeta_x \sin\varphi_i + \zeta_y \cos\varphi_i) \\ \left[\begin{array}{c} \underline{e}_x(\sin\vartheta_i \cos\varphi_i + \zeta_x \cos\vartheta_i) \\ +\underline{e}_y(\sin\vartheta_i \sin\varphi_i + \zeta_y \cos\vartheta_i) \\ +\underline{e}_z(\zeta_x \sin\vartheta_i \cos\varphi_i + \zeta_y \sin\vartheta_i \sin\varphi_i) \end{array}\right] \end{array}\right\} e^{-ikr}
\tag{65}
$$

and for the electric currents,

$$\begin{aligned}\underline{e}_n \times H^{inc} &= \frac{1}{\eta_0}\left[\underline{e}_x \cos\varphi_i + \underline{e}_y \sin\varphi + \underline{e}_z(\zeta_x \cos\varphi_i + \zeta_y \sin\varphi_i)\right] e^{-ikr} \\ \underline{H}^{inc} \cdot \underline{e}_T &= \frac{1}{\eta_0}\left(\sin\vartheta_i + \zeta_x \cos\vartheta_i \cos\varphi_i + \zeta_y \cos\vartheta_i \sin\varphi_i\right) e^{-ikr}\end{aligned} \tag{66}$$

and substituting (66) into (61) gives

$$\underline{J} = \left\{ \begin{array}{c} (1 - R_{TE})[\underline{e}_x \cos\varphi_i + \underline{e}_y \sin\varphi_i \\ \qquad + \underline{e}_z(\zeta_x \cos\varphi_i + \zeta_y \sin\varphi_i)] \\ +(R_{TE} + R_{TM})(\sin\vartheta_i + \zeta_x \cos\vartheta_i \cos\varphi_i \\ \qquad + \zeta_y \cos\vartheta_i \sin\varphi_i) \\ \left[\begin{array}{c} \underline{e}_x(\sin\vartheta_i \cos\varphi_i + \zeta_x \cos\vartheta_i) \\ +\underline{e}_y(\sin\vartheta_i \sin\varphi_i + \zeta_y \cos\vartheta_i) \\ +\underline{e}_z(\zeta_x \sin\vartheta_i \cos\varphi_i + \zeta_y \sin\vartheta_i \sin\varphi_i) \end{array} \right] \end{array} \right\} \frac{e^{-ikr}}{\eta_0} \tag{67}$$

Substituting (67) in (54) gives

$$
\underline{\underline{\Gamma}} \cdot \underline{J} =
$$

$$
\left\{
\begin{array}{l}
(1 - R_{TE}) \left[
\begin{array}{r}
\underline{e}_x(\cos\varphi_i \cos^2\vartheta_i - \sin\vartheta_i \cos\vartheta_i \cos\varphi_i \\
\{\zeta_x \cos\varphi_i + \zeta_y \sin\varphi_i\}) \\
+\underline{e}_y(\sin\varphi_i \cos^2\vartheta_i - \sin\vartheta_i \cos\vartheta_i \sin\varphi_i \\
\{\zeta_x \cos\varphi_i + \zeta_y \sin\varphi_i\}) \\
+\underline{e}_z(-\sin\vartheta_i \cos\vartheta_i + \sin^2\vartheta_i \\
\{\zeta_x \cos\varphi_i + \zeta_y \sin\varphi_i\})
\end{array}
\right] \\
+(R_{TE} + R_{TM})(\sin\vartheta_i + \cos\vartheta_i \\
\{\zeta_x \cos\varphi_i + \zeta_y \sin\varphi_i\}) \\
\cdots \left[
\begin{array}{c}
\underline{e}_x(\sin\vartheta_i \cos^2\vartheta_i \cos\varphi_i \\
+\zeta_x \cos\vartheta_i \{1 - 2\sin^2\vartheta_i \cos^2\varphi_i\} \\
-2\zeta_y \sin^2\vartheta_i \cos\vartheta_i \sin\varphi_i \cos\varphi) \\
+\underline{e}_y(\sin\vartheta_i \cos^2\vartheta_i \sin\varphi_i \\
+\zeta_y \cos\vartheta_i \{1 - 2\sin^2\vartheta_i \sin^2\varphi_i\} \\
-2\zeta_x \sin^2\vartheta_i \cos\vartheta_i \sin\varphi_i \cos\varphi_i) \\
+\underline{e}_z(-\sin^2\vartheta_i \cos\vartheta_i \\
+\sin\vartheta_i \{1 - 2\cos^2\vartheta_i\} \{\zeta_x \cos\varphi_i \\
+\zeta_y \sin\varphi_i\})
\end{array}
\right]
\end{array}
\right\} \tag{68}
$$

$$
\cdots \frac{e^{-ikr}}{\eta_0} \frac{e^{ikR}}{4\pi R}
$$

Substituting (65) into (64) gives

$$\underline{K} \times \underline{\nabla}' G =$$

$$\left\{ \begin{array}{l} (1 - R_{TM}) \left[\begin{array}{c} \underline{e}_x(-\cos^2\vartheta_i \cos\varphi_i \\ +\sin\vartheta_i \cos\vartheta_i \cos\varphi_i\{\zeta_x \cos\varphi_+ \zeta_y \sin\varphi_i\}) \\ +\underline{e}_y(-\cos^2\vartheta_i \sin\varphi_i \\ +\sin\vartheta_i \cos\vartheta_i \sin\varphi_i\{\zeta_x \cos\varphi_i + \zeta_y \sin\varphi_i\} \\ +\underline{e}_z(\sin\vartheta_i \cos\vartheta \\ -\sin^2\vartheta_i\{\zeta_x \cos\varphi_i + \zeta_y \sin\varphi_i\}) \end{array} \right] \\ (R_{TE} + R_{TM}) \left[\begin{array}{c} \underline{e}_x(\sin\vartheta_i \cos\vartheta_i \sin\varphi_i\{\zeta_x \sin\varphi_i - \zeta_y \cos\varphi_i\}) \\ +\underline{e}_y(\sin\vartheta_i \cos\vartheta_i \cos\varphi_i\{-\zeta_x \sin\varphi_i + \zeta_y \cos\varphi_i\} \end{array} \right] \end{array} \right\} \cdot$$

$$\cdots (-ik) \frac{e^{-ikr+ikR}}{4\pi R} \tag{69}$$

Combining the two terms in the integrand of (54) gives

$$ik\eta_0 \underline{\underline{\Gamma}} \cdot \underline{J} + \underline{K} \times \underline{\nabla}' G = \frac{e^{-ik(r-R)}}{4\pi R} \cdot$$

$$\left\{ \begin{array}{l} \underline{e}_x \left[\begin{array}{c} 2\cos^2\vartheta_i \cos\varphi_i \\ -2\sin\vartheta_i \cos\vartheta_i \cos\varphi_i\{\zeta_x \cos\varphi_i + \zeta_y \sin\varphi_i\} \\ -(R_{TE} + R_{TM}) \cos^3\vartheta_i \cos\varphi_i\{\cos\vartheta_i \\ -3\sin\vartheta_i[\zeta_x \cos\varphi_i + \zeta_y \sin\varphi_i]\} \end{array} \right] \\ +\underline{e}_y \left[\begin{array}{c} 2\cos^2\vartheta_i \sin\varphi_i \\ -2\sin\vartheta_i \cos\vartheta_i \sin\varphi_i\{\zeta_x \cos\varphi_i + \zeta_y \sin\varphi_i\} \\ -(R_{TE} + R_{TM}) \cos^3\vartheta_i \sin\varphi_i\{\cos\vartheta_i \\ -3\sin\vartheta_i[\zeta_x \cos\varphi_i + \zeta_y \sin\varphi_i]\} \end{array} \right] \\ +\underline{e}_z \left[\begin{array}{c} -2\sin\vartheta_i \cos\vartheta_i \\ +2\sin^2\vartheta_i\{\zeta_x \cos\varphi_i + \zeta_y \sin\varphi_i\} \\ +(R_{TE} + R_{TM}) \sin\vartheta_i \cos^2\vartheta_i\{\cos\vartheta_i \\ -3\sin\vartheta_i[\zeta_x \cos\varphi_i + \zeta_y \sin\varphi_i]\} \end{array} \right] \end{array} \right\} \tag{70}$$

The final expression for the scattered TM field is

$$\begin{aligned}\underline{E}^s_{TM}(x,y,z) = 2\underline{e}_\vartheta \frac{(-ik)e^{ikr}}{4\pi r}\int_{x_1}^{x_2} dx' \int_{y_1}^{y_2} dy' \\ \cdots e^{-i2k(x'\sin\vartheta_i\cos\varphi_i + y'\sin\vartheta_i\sin\varphi_i + z'\cos\vartheta_i)} \\ \cdots \left\{ \begin{array}{c} \cos\vartheta_i - \sin\vartheta_i(\zeta_x\cos\varphi_i + \zeta_y\sin\varphi_i) \\ -\frac{1}{2}(R_{TE}+R_{TM})\cos^2\vartheta_i \\ [\cos\vartheta_i - 3\sin\vartheta_i(\zeta_x\cos\varphi_i + \zeta_y\sin\varphi_i)] \end{array} \right\}\end{aligned} \tag{71}$$

and for the case of a perfectly conducting surface, where

$$\begin{aligned} R_{TE} &\overrightarrow{\sigma\to\infty} -1 \\ R_{TM} &\overrightarrow{\sigma\to\infty} +1 \end{aligned} \tag{72}$$

the result in (71) reduces to the result derived by Collin (1992). For the case of grazing incidence, (71) reduces to the perturbation result given by Ott, et al. (1973).

The TE case is now presented, even though it does not differ from the derivation for the TM case because, it is important to show the backscattered field has the correct polarization dependence at grazing incidence.

$$\begin{aligned}\underline{e}_n \times \underline{E}^{inc} &= \left(-\zeta_x \underline{e}_x - \zeta_y \underline{e}_y + \underline{e}_z\right) \times \left(-\underline{e}_x \sin\varphi_i + \underline{e}_y \cos\varphi_i\right) \\ &\quad \cdots e^{-ik(x' \sin\vartheta_i \cos\varphi_i + y' \sin\vartheta_i \sin\varphi_i + z' \cos\vartheta_i)} \\ &= -\left[\underline{e}_x \cos\varphi_i + \underline{e}_y \sin\varphi_i + \underline{e}_z \left(\zeta_x \cos\varphi_i + \zeta_y \sin\varphi_i\right)\right] \\ &\quad \cdots e^{-ik(x' \sin\vartheta_i \cos\varphi_i + y' \sin\vartheta_i \sin\varphi_i + z' \cos\vartheta_i)}\end{aligned}$$

$$\begin{aligned}\underline{E}^{inc} \cdot \underline{e}_T &= (-\underline{e}_x \sin\varphi_i + \underline{e}_y \cos\varphi_i) \cdot \\ &\qquad \begin{bmatrix} \underline{e}_x(\sin\vartheta_i \sin\varphi_i + \zeta_y \cos\vartheta_i) \\ +\underline{e}_y(-\sin\vartheta_i \cos\varphi_i - \zeta_x \cos\vartheta_i) \\ +\underline{e}_z \sin\vartheta_i(\zeta_x \sin\varphi_i - \zeta_y \cos\varphi_i) \end{bmatrix} \\ &\quad \cdots e^{-ik(x' \sin\vartheta_i \cos\varphi_i + y' \sin\vartheta_i \sin\varphi_i + z' \cos\vartheta_i)} \\ &= -\left[\sin\vartheta_i + \cos\vartheta_i \left(\zeta_x \cos\varphi_i + \zeta_y \sin\varphi_i\right)\right] \\ &\quad \cdots e^{-ik(x' \sin\vartheta_i \cos\varphi_i + y' \sin\vartheta_i \sin\varphi_i + z' \cos\vartheta_i)}\end{aligned} \tag{73}$$

and,

$$\begin{aligned}\left(\underline{E}^{inc} \cdot \underline{e}_T\right)\left[\underline{e}_R - \underline{e}_n(\underline{e}_R \cdot \underline{e}_n)\right] &= -\left[\sin\vartheta_i + \cos\vartheta_i(\zeta_x \cos\varphi_i + \zeta_y \sin\varphi_i)\right] \\ &\quad \cdots \left\{ \begin{array}{c} \underline{e}_x[\sin\vartheta_i \cos\varphi_i + \zeta_x \cos\vartheta_i] \\ +\underline{e}_y[\sin\vartheta_i \sin\varphi_i + \zeta_y \cos\vartheta_i] \\ +\underline{e}_z \sin\vartheta_i(\zeta_x \cos\varphi_i + \zeta_y \sin\varphi_i) \end{array} \right\} \\ &\quad \cdots e^{-ik(x' \sin\vartheta_i \cos\varphi_i + y' \sin\vartheta_i \sin\varphi_i + \cos\vartheta_i)} \\ &= -\left[\sin\vartheta_i + \cos\vartheta_i(\zeta_x \cos\varphi_i + \zeta_y \sin\varphi_i)\right] \\ &\quad \cdots \left\{ \begin{array}{c} \underline{e}_x[\sin\vartheta_i \cos\varphi_i + \zeta_x \cos\vartheta_i] \\ +\underline{e}_y[\sin\vartheta_i \sin\varphi_i + \zeta_y \cos\vartheta_i] \\ +\underline{e}_z \sin\vartheta_i(\zeta_x \cos\varphi_i + \zeta_y \sin\varphi_i) \end{array} \right\} \\ &\quad \cdots e^{-ik(x' \sin\vartheta_i \cos\varphi_i + y' \sin\vartheta_i \sin\varphi_i + z' \cos\vartheta_i)}\end{aligned} \tag{74}$$

Substituting (73) and (74) into (61) gives

$$\underline{K} = \left\{ \begin{array}{c} (1-R_{TM})\Big[\underline{e}_x \cos\varphi_i + \underline{e}_y \sin\varphi_i \\ +\underline{e}_z(\zeta_x \cos\varphi_i + \zeta_y \sin\varphi_i)\Big] \\ +(R_{TE}+R_{TM})\Big[\sin\vartheta_i \\ +\cos\vartheta_i(\zeta_x\cos\varphi_i + \zeta_y \sin\varphi_i)\Big] \\ \left[\begin{array}{c} \underline{e}_x(\sin\vartheta_i\cos\varphi_i + \zeta_x\cos\vartheta_i) \\ +\underline{e}_y(\sin\vartheta_i\sin\varphi_i + \zeta_y\cos\vartheta_i) \\ +\underline{e}_z\sin\vartheta_i(\zeta_x\cos\varphi_i + \zeta_y\sin\varphi_i) \end{array}\right] \end{array} \right\}$$

$$\cdots e^{-ik(x'\sin\vartheta_i\cos\varphi_i + y'\sin\vartheta_i\sin\varphi_i + z'\cos\vartheta_i)}.$$

$$= \left\{ \begin{array}{c} \underline{e}_x\Big[\cos\varphi_i(1-R_{TM}) + (R_{TE}+R_{TM})\sin\vartheta_i \\ \left(\begin{array}{c} \sin\vartheta_i\cos\varphi_i + \zeta_x\cos\vartheta_i + \\ \cos\vartheta_i\cos\varphi_i\{\zeta_x\cos\varphi_i + \zeta_y\sin\varphi_i\} \end{array}\right)\Big] \\ +\underline{e}_y\Big[\sin\varphi_i(1-R_{TM}) + (R_{TE}+T_{TM})\sin\vartheta_i \\ \left(\begin{array}{c} \sin\vartheta_i\sin\varphi_i + \zeta_y\cos\vartheta_i + \\ \cos\vartheta_i\sin\varphi_i\{\zeta_x\cos\varphi_i + \zeta_y\sin\varphi_i\} \end{array}\right)\Big] \\ +\underline{e}_z[\,(\zeta_x\cos\varphi_i + \zeta_y\sin\varphi_i)\,(1-R_{TM}) \\ +(R_{TE}+R_{TM})\sin^2\vartheta_i(\zeta_x\cos\varphi_i + \zeta_y\sin\varphi_i)] \end{array} \right\}.$$

$$\cdots e^{-ik(x'\sin\vartheta_i\cos\varphi_i + y'\sin\vartheta_i\sin\varphi_i + z'\cos\vartheta_i)} \tag{75}$$

Substituting (75) into (54)

$$\underline{K} \times \underline{\nabla}' G =$$

$$(-ik)\,\frac{e^{ikR}}{4\pi R}\left\{\begin{array}{c} \underline{e}_x\Big[\cos\varphi_i\,(1-R_{TM})+(R_{TE}+R_{TM})\sin\vartheta_i \\ \left(\begin{array}{c}\sin\vartheta_i\cos\varphi_i+\zeta_x\cos\vartheta_i \\ +\cos\vartheta_i\cos\varphi_i\left\{\zeta_x\cos\varphi_i+\zeta_y\sin\varphi_i\right\}\end{array}\right)\Big] \\ +\underline{e}_y\Big[\sin\varphi_i\,(1-R_{TM})+(R_{TE}+R_{TM})\sin\vartheta_i \\ \left(\begin{array}{c}\sin\vartheta_i\sin\varphi_i+\zeta_y\cos\vartheta_i \\ +\cos\vartheta_i\sin\varphi_i\left\{\zeta_x\cos\varphi_i+\zeta_y\sin\varphi_i\right\}\end{array}\right)\Big] \\ +\underline{e}_z\Big(\zeta_x\cos\varphi_i+\zeta_y\sin\varphi_i\Big) \\ \Big[(1-R_{TM})+(R_{TE}+R_{TM})\sin^2\vartheta_i\Big] \end{array}\right\}$$

$$\times\left(\underline{e}_x\sin\vartheta_i\cos\varphi+\underline{e}_y\sin\vartheta_i\sin\varphi_i+\underline{e}_z\cos\vartheta_i\right)$$

$$\cdots e^{-ik(x'\sin\vartheta_i\cos\varphi_i+y'\sin\vartheta_i\sin\varphi_i+z'\cos\vartheta_i)}$$

$$=\left\{\begin{array}{l} \underline{e}_x\left[\begin{array}{c}\cos\vartheta_i\sin\varphi_i\,(1-R_{TM})-\sin\vartheta_i\sin\varphi_i \\ (\zeta_x\cos\varphi_i+\zeta_y\sin\varphi_i)\,(1-R_{TM}) \\ +(R_{TE}+R_{TM})\sin\vartheta_i \\ \Big(\sin\vartheta_i\cos\vartheta_i\sin\varphi_i+\zeta_y\cos^2\vartheta_i+ \\ \left(\sin\varphi_i\left\{\zeta_x\cos\varphi_i+\zeta_y\sin\varphi_i\right\}\left\{\cos^2\vartheta_i-\sin^2\vartheta_i\right\}\right)\end{array}\right] \\ +\underline{e}_y\left[\begin{array}{c}-\cos\vartheta_i\cos\varphi_i\,(1-R_{TM})+\sin\vartheta_i\cos\varphi_i \\ (\zeta_x\cos\varphi_i+\zeta_y\sin\varphi_i)\,(1-R_{TM}) \\ -(R_{TE}+R_{TM})\sin\vartheta_i \\ \Big(\sin\vartheta_i\cos\vartheta_i\cos\varphi_i+\zeta_x\cos^2\vartheta_i+ \\ \left(\cos\varphi_i\left\{\zeta_x\cos\varphi_i+\zeta_y\sin\varphi_i\right\}\left\{\cos^2\vartheta_i-\sin^2\vartheta_i\right\}\right)\end{array}\right] \\ -\underline{e}_z\,(R_{TE}+R_{TM})\sin^2\vartheta_i\cos\vartheta_i\,(\zeta_y\cos\varphi_i-\zeta_x\sin\varphi_i) \end{array}\right\}$$

$$\cdots(-ik)\,\frac{e^{ikR-ik(x'\sin\vartheta_i\cos\varphi_i+y'\sin\vartheta_i\sin\varphi_i+z'\cos\vartheta_i)}}{4\pi R} \tag{76}$$

For the electric current,

$$\begin{aligned}
\underline{e}_n \times \underline{H}^{inc} &= \left(-\zeta_x \underline{e}_x - \zeta_y \underline{e}_y + \underline{e}_z\right) \\
&\quad \times \left(\underline{e}_x \cos\vartheta_i \cos\varphi_i + \underline{e}_y \cos\vartheta_i \sin\varphi_i - \underline{e}_z \sin\vartheta_i\right) \\
&\quad \cdots \frac{e^{-ik(x' \sin\vartheta_i \cos\varphi_i + y' \sin\vartheta_i \sin\varphi_i + z' \cos\vartheta_i)}}{\eta_0} \\
&= \begin{bmatrix} -\underline{e}_x \left(\cos\vartheta_i \sin\varphi_i - \zeta_y \sin\vartheta_i\right) \\ +\underline{e}_y \left(\cos\vartheta_i \cos\varphi_i - \zeta_x \sin\vartheta_i\right) \\ -\underline{e}_z \cos\vartheta_i \left(\zeta_x \sin\varphi_i - \zeta_y \cos\varphi_i\right) \end{bmatrix} \\
&\quad \cdots \frac{1}{\eta_0} e^{-ik(x' \sin\vartheta_i \cos\varphi_i + y' \sin\vartheta_i \sin\varphi_i + z' \cos\vartheta_i)}
\end{aligned} \tag{77}$$

$$\begin{aligned}
&\underline{H}^{inc} \cdot \underline{e}_T = \\
&\quad -(\zeta_x \sin\varphi_i - \zeta_y \cos\varphi_i) \frac{1}{\eta_0} e^{-ik(x' \sin\vartheta_i \cos\varphi_i + y' \sin\vartheta_i \sin\varphi_i + z' \cos\vartheta_i)} \\
&\underline{J} = \left\{ \begin{array}{l}
\underline{e}_x \begin{bmatrix} -(1 - R_{TE}) \left(\cos\vartheta_i \sin\varphi_i - \zeta_y \sin\vartheta_i\right) \\ + \left(R_{TE} + R_{TM}\right) \cdot \\ \cdots \left(\sin\vartheta_i \cos\varphi_i + \zeta_x \cos\vartheta_i\right) \\ \left(\zeta_y \cos\varphi_i - \zeta_x \sin\varphi_i\right) \end{bmatrix} \\
\underline{e}_y \begin{bmatrix} (1 - R_{TE}) \left(\cos\vartheta_i \cos\varphi_i - \zeta_x \sin\vartheta_i\right) \\ + \left(R_{TE} + R_{TM}\right) \cdot \\ \cdots \left(\sin\vartheta_i \sin\varphi_i + \zeta_y \cos\vartheta_i\right) \\ \left(\zeta_y \cos\varphi_i - \zeta_x \sin\varphi_i\right) \end{bmatrix} \\
+\underline{e}_z \begin{bmatrix} (1 - R_{TE}) \cos\vartheta_i \left(\zeta_y \cos\varphi_i - \zeta_x \sin\varphi_i\right) \\ + \left(R_{TE} + R_{TM}\right) \cdot \\ \cdots \sin\vartheta_i \left(\zeta_y \cos\varphi_i - \zeta_x \sin\varphi_i\right) \\ \left(\zeta_x \cos\varphi_i + \zeta_y \sin\varphi_i\right) \end{bmatrix}
\end{array} \right\} \cdot \\
&\quad \cdots \frac{1}{\eta_0} e^{-ik(x' \sin\vartheta_i \cos\varphi_i + y' \sin\vartheta_i \sin\varphi_i + z' \cos\vartheta_i)}
\end{aligned} \tag{78}$$

Substituting (78) into (54)

$$ik\eta_0 \underline{\underline{\Gamma}} \cdot \underline{J} = \left\{ \begin{array}{c} \underline{e}_x \left[\begin{array}{c} -(1-R_{TE}) \sin\varphi_i (\cos\vartheta_i \\ -\sin\vartheta_i \{\zeta_x \cos\varphi_i + \zeta_y \sin\varphi_i\}) \\ +(R_{TE}+R_{TM}) \sin\vartheta_i \cos^2\vartheta_i \\ \cos\varphi_i (\zeta_y \cos\varphi_i - \zeta_x \sin\varphi_i) \end{array} \right] \\ +\underline{e}_y \left[\begin{array}{c} (1-R_{TE}) \cos\varphi_i (\cos\vartheta_i \\ -\sin\vartheta_i \{\zeta_x \cos\varphi_i + \zeta_y \sin\varphi_i\}) \\ +(R_{TE}+R_{TM}) \sin\vartheta_i \cos^2\vartheta_i \\ \sin\varphi_i (\zeta_y \cos\varphi_i - \zeta_x \sin\varphi_i) \end{array} \right] \\ +\underline{e}_z \Big[-(R_{TE}+R_{TM}) \sin^2\vartheta_i \\ \cos\vartheta_i (\zeta_y \cos\varphi_i - \zeta_x \sin\varphi_i) \Big] \end{array} \right\} \tag{79}$$

$$\cdots \frac{(ik)\, e^{ikR - ik(x' \sin\vartheta_i \cos\varphi_i + y' \sin\vartheta_i \sin\varphi_i + z' \cos\vartheta_i)}}{4\pi R}$$

Combining (79) and (76) gives

$$ik\eta_0 \underline{\underline{\Gamma}} \cdot \underline{J} + \underline{K} \times \underline{\nabla}' G =$$

$$\frac{(ik)\, e^{ikR - ik(x' \sin\vartheta_i \cos\varphi_i + y' \sin\vartheta_i \sin\varphi_i + z' \cos\vartheta_i)}}{4\pi R} \cdot$$

$$\cdots \left\{ \begin{array}{c} \underline{e}_x \left[\begin{array}{c} -\sin\varphi_i (\cos\vartheta_i - \sin\vartheta_i \{\zeta_x \cos\varphi_i + \zeta_y \sin\varphi_i\}) \\ (2-(R_{TE}+R_{TM})) + (R_{TE}+R_{TM}) \sin\vartheta_i) \\ \left(\begin{array}{c} \cos^2\vartheta_i \cos\varphi_i \{\zeta_y \cos\varphi_i - \zeta_x \sin\varphi_i\} \\ -\sin\vartheta_i \cos\vartheta_i \sin\varphi_i \\ -\zeta_y \cos^2\vartheta_i - \sin\varphi_i \\ \{\zeta_x \cos\varphi_i + \zeta_y \sin\varphi_i\} \{\cos^2\vartheta_i - \sin^2\vartheta_i\} \end{array} \right) \end{array} \right] \\ +\underline{e}_y \left[\begin{array}{c} \cos\varphi_i (\cos\vartheta_i - \sin\vartheta_i \{\zeta_x \cos\varphi_i + \zeta_y \sin\varphi_i\}) \\ (2-(R_{TE}+R_{TM})) + (R_{TE}+R_{TM}) \sin\vartheta_i \\ \left(\begin{array}{c} \cos^2\vartheta_i \sin\varphi_i \{\zeta_y \cos\varphi_i - \zeta_x \sin\varphi_i\} \\ +\sin\vartheta_i \cos\vartheta_i \cos\varphi_i \\ +\zeta_x \cos^2\vartheta_i + \cos\varphi_i \{\zeta_x \cos\varphi_i + \zeta_y \sin\varphi_i\} \\ \{\cos^2\vartheta_i - \sin^2\vartheta_i\} \end{array} \right) \end{array} \right] \end{array} \right\} \tag{80}$$

and simplifying,

$$
\begin{aligned}
ik\eta_0 \underline{\underline{\Gamma}} \cdot \underline{K} \times \underline{\nabla}' G + &= \frac{(ik)\, e^{ikR-(x' \sin\vartheta_i \cos\varphi_i + y' \sin\vartheta_i \sin\varphi_i + z' \cos\vartheta_i)}}{4\pi R} \cdot \\
\cdots &\left\{ \begin{array}{c} -\underline{e}_x \left[\begin{array}{c} 2 \sin\varphi_i \cos\vartheta_i \\ -2 \sin\vartheta_i \sin\varphi_i (\zeta_x \cos\varphi_i + \zeta_y \sin\varphi_i) \\ -(R_{TE} + R_{TM}) \cos^2\vartheta_i \sin\varphi_i \\ (\cos\vartheta_i - 3 \sin\vartheta_i \, (\zeta_x \cos\varphi_i + \zeta_y \sin\varphi)) \end{array} \right] \\ +\underline{e}_y \left[\begin{array}{c} 2 \cos\varphi_i \cos\vartheta_i \\ 2 \cos\varphi_i \cos\vartheta_i - 2 \cos\varphi_i \sin\vartheta_i \, (\zeta_x \cos\varphi_i + \zeta_y \sin\varphi_i) \\ -(R_{TE} + R_{TM}) \cos^2\vartheta_i \cos\varphi_i \\ (\cos\vartheta_i - 3 \sin\vartheta_i \, (\zeta_x \cos\varphi_i + \zeta_y \sin\varphi_i)) \end{array} \right] \end{array} \right\} \\
&= \frac{(ik)\, e^{ikR - ik(x' \sin\vartheta_i \cos\varphi_i + y' \sin\vartheta_i \sin\varphi_i + z' \cos\vartheta_i)}}{4\pi R} \cdot \\
\cdots &\, \underline{e}_\varphi \left\{ \begin{array}{c} 2 \left[\cos\vartheta_i - \sin\vartheta_i \, (\zeta_x \cos\varphi_i + \zeta_y \sin\varphi_i) \right] \\ -(R_{TE} + R_{TM}) \cos^2\vartheta_i \\ \left[\cos\vartheta_i - 3 \sin\vartheta_i (\zeta_x \cos\varphi_i + \zeta_y \sin\varphi_i) \right] \end{array} \right\}
\end{aligned}
\tag{81}
$$

and the final result for the TE case is

$$
\begin{aligned}
&\underline{E}^s_{TE}(x, y, z) = \\
&\quad \underline{e}_\varphi \frac{2(ik) e^{ikr}}{4\pi R} \int_{x_1}^{x_2} dx' \int_{y_1}^{y_2} dy' e^{-2ik(x' \sin\vartheta_i \cos\varphi_i + y' \sin\vartheta_i \sin\varphi_i + z' \cos\vartheta_i)} \cdot \\
&\cdots \left\{ \begin{array}{c} \cos\vartheta_i - \sin\vartheta_i \, (\zeta_x \cos\varphi_i + \zeta_y \sin\varphi_i) \\ -\frac{1}{2}(R_{TE} + R_{TM}) \cos^2\vartheta_i \\ \left[\cos\vartheta_i - 3 \sin\vartheta_i (\zeta_x \cos\varphi_i + \zeta_y \sin\varphi_i) \right] \end{array} \right\}
\end{aligned}
\tag{82}
$$

This section is concluded by showing the details of the derivation for Collin's result for the case of a perfectly conducting rough surface. Starting from Colin's Equation (36) with two proper rotations of his coordinate frame to bring it into agreement with Figure 4, i.e., making the replacements:

$$\begin{aligned} x_{Collin} &\rightarrow y \\ y_{Collin} &\rightarrow z \\ z_{Collin} &\rightarrow x \end{aligned} \tag{83}$$

Then Collin's Equation (36) can be written as

$$\begin{aligned} \underline{E}^s_{TM}(x,y,z) = \frac{-2jk_0}{(2\pi)^3}\int_0^\infty dk_z \int_{-\infty}^\infty dk_y \int_{-\infty}^\infty dk_x \int_{x_1}^{x_2} dx' \int_{y_1}^{y_2} dy' \\ \cdots \frac{(\underline{k}\times\underline{k}\times\underline{e}_z)(\underline{k}\times\underline{k}\times\underline{e}_z)\cdot\underline{J}_e}{k^2(k^2-k_0^2)(k_x^2+k_y^2)} \\ \cdots e^{j(k_z^{inc}+k_z)\zeta + j(k_y-k_y^{inc})y' + j(k_x-k_x^{inc})x' - j(k_x x + k_y y + k_z z)} \end{aligned} \tag{84}$$

which has poles at

$$\begin{aligned} &k = \pm k_0 \qquad or \qquad k_x = \pm(k_0^2 - k_y^2 - k_z^2)^{1/2} \\ &\text{and} \\ &k_x = \pm j k_y \end{aligned} \tag{85}$$

If the path of integration in Figure 5 is closed in the upper-half of the complex k_x plane, and assuming a small loss in k_0 so that the poles are off the real axis and the integral is well-defined, as in Figure 5, then the residue at the pole at k_x is

$$2\pi j \frac{1}{(k_x^2+k_y^2)}\frac{1}{2k_x} = \frac{\pi j}{(k_0^2-k_z^2)k_x} \tag{86}$$

and the residue at the pole at jk_y is

$$2\pi j \frac{1}{(k^2-k_0^2)}\frac{1}{2jk_y} = \frac{-\pi j}{(k_z^2-k_0^2)k_x} \tag{87}$$

and the total residue from both poles is

$$\frac{2\pi j}{(k_0^2-k_z^2)k_x} \tag{88}$$

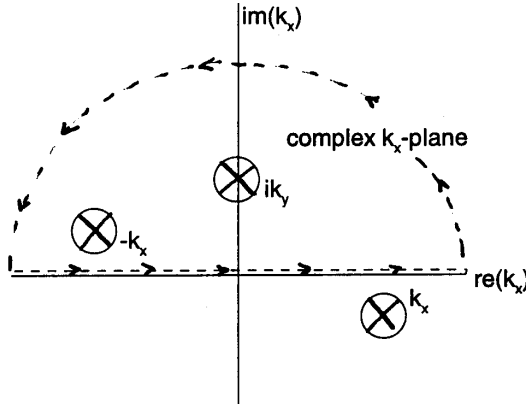

Figure 5. Path of integration in the complex k_x-plane.

Next, stationary phase integration is applied to the integrations on k_y and k_z with

$$\begin{aligned} I &= \int_0^\infty dk_z \int_{-\infty}^\infty dk_y e^{-j(k_y y + k_z z) - j\sqrt{k_0^2 - k_y^2 - k_z^2}\,x} \\ \frac{\partial g}{\partial k_y} &: -y + \frac{k_y x}{\sqrt{k_0^2 - k_y^2 - k_z^2}} = 0 \\ \frac{\partial g}{\partial k_z} &: -z + \frac{k_z x}{\sqrt{k_0^2 - k_y^2 - k_z^2}} = 0 \end{aligned} \tag{89}$$

$$g = k_y y + k_z z + x\sqrt{k_x^2 + k_y^2 - k_z^2}$$

and solving for k_y, k_z gives

$$\begin{aligned} \frac{k_y}{k_z} &= \pm\frac{y}{z} = \pm\frac{\sin\vartheta_s \sin\varphi_s}{\cos\vartheta_s} \\ k_x &= k_0 \sin\vartheta_s \cos\varphi_s \end{aligned} \tag{90}$$

and in the backscatter direction,

$$\begin{aligned} \varphi_s &= \pi + \varphi_i \\ \vartheta_s &= \vartheta_i \\ \sin\varphi_i &= -\sin\varphi_s \\ \cos\varphi_i &= -\cos\varphi_s \end{aligned} \tag{91}$$

The second derivatives of the phase of the integral in Equation (89) are given by

$$\begin{aligned}\frac{\partial^2 g}{\partial k_y^2} &= \frac{x(k_0^2 - k_z^2)}{(k_0^2 - k_y^2 - k_z^2)^{3/2}} \\ \frac{\partial^2 g}{\partial k_z^2} &= \frac{x(k_0^2 - k_y^2)}{(k_0^2 - k_y^2 - k_z^2)^{3/2}} \\ \frac{\partial^2 g}{\partial k_y \partial k_z} &= \frac{x k_y k_z}{(k_0^2 - k_y^2 - k_z^2)^{3/2}}\end{aligned} \tag{92}$$

and the amplitude of the stationary phase integration gives

$$\begin{aligned}&\frac{2\pi j}{\sqrt{\frac{\partial^2 gf}{\partial k_y^2}\frac{\partial^2 gf}{\partial k_z^2} - \left(\frac{\partial^2 gf}{\partial k_y \partial k_z}\right)^2}} = \\ &\frac{2\pi j}{\frac{r\sin\vartheta_s\cos\varphi_s}{k_0^3\sin\vartheta_s\cos\varphi_s} k_0^4 \sqrt{\sin^2\vartheta_s(1 - \sin^2\vartheta_s\sin^2\varphi_s) - \sin^2\vartheta_s\cos^2\vartheta_s\sin^2\varphi_s}} \\ &\quad = \frac{2\pi j k_0 \sin\vartheta_s\cos^2\varphi_s}{r\sqrt{1 - \sin^2\vartheta_s\sin^2\varphi_s - \cos^2\vartheta_s\sin^2\varphi_s}} \\ &\quad = \frac{2\pi j k_0 \sin\vartheta_s\cos\varphi_s}{r} \\ &\quad = \frac{2\pi j k_x}{r}\end{aligned} \tag{93}$$

and multiplying (93) by the residue is (88) gives

$$\frac{-(2\pi)^2}{r k_0^2 \sin^2\vartheta_s} \tag{94}$$

The dyad in the integrand in Equation (84) is

$$\begin{aligned}&\underline{k} = k_0(\underline{e}_x \sin\vartheta_i\cos\varphi_i + \underline{e}_y \sin\vartheta_i \sin\varphi_i + \underline{e}_z\cos\vartheta_i) \\ &\underline{k}\times\underline{e}_z = k_0(-\underline{e}_y\sin\vartheta_i\cos\varphi_i + \underline{e}_x\sin\vartheta_i\sin\varphi_i) \\ &\underline{k}\times\underline{k}\times\underline{e}_z = k_0^2\sin\vartheta_i(\underline{e}_x\cos\vartheta_i\cos\varphi_i + \underline{e}_y\cos\vartheta_i\sin\varphi_i - \underline{e}_z\sin\vartheta_i) \\ &\qquad\qquad = k_0^2\sin\vartheta_i\underline{e}_\vartheta \\ &\underline{J}_e = \underline{e}_x\cos\varphi_i + \underline{e}_y\sin\varphi_i + \underline{e}_z(\zeta_x\cos\varphi_i + \zeta_y\sin\varphi_i) \\ &(\underline{k}\times\underline{k}\times\underline{e}_z)\cdot\underline{J}_e = k_0^2\sin\vartheta_i[\cos\vartheta_i - \sin\vartheta_i(\zeta_x\cos\varphi_i + \zeta_y\sin\varphi_i)]\end{aligned} \tag{95}$$

and the final result for the integral in (84) becomes

$$\begin{aligned}\underline{E}^S_{TM}(x,y,z) = \frac{-jk_0}{2\pi}\left(\frac{e^{ikr}}{r}\right)\underline{e}_\vartheta \int_{x_1}^{x_2} dx' \int_{y_1}^{y_2} dy' \\ \cdot \Big[\cos\vartheta_i - \sin\vartheta_i(\zeta_x\cos\varphi_i + \zeta_y \sin\varphi_i)\Big] \\ \cdots e^{2jk_0(x'\sin\vartheta_i\cos\varphi_i + y'\sin\vartheta_i\sin\varphi_i + \zeta\cos\vartheta_i)}\end{aligned} \tag{96}$$

in agreement with Equation (71).

10. Examples of EM Backscatter from Buried Targets

The frequency band is an important consideration in the detection of buried targets (Peters, et al., 1994). Scattering results are computed for two bands: 1) 10–500 MHz and 2) 300–800 MHz. The trade-off in frequency bands is important because the lower band has small antenna gain with better ground penetration while at the higher band the opposite is true. In air-borne SAR applications when low gain antennas are used causing a large patch of ground to be illuminated, the clutter from the interface is large (as much as 60 dB greater than the target return). Coherent integration of thousands of pulses is required to acheive the necessary processing gain to offset the difference between the interface and target returns. The best way to appreciate the trade-off in the choice of frequency band is to perform a power budget for each, using the values for the target and interface scatter generated from the analysis of the preceding sections.

Figure 4 shows the plot of a sample 3-D terrain profile. Having 10 segments of one meter length in both the x- and y-direction, this is the surface used to simulate the 3-D rough surface scatter. Figure 6 shows a "waterfall" plot of the scattered power versus ϑ in degrees, where zero corresponds to normal incidence and time in μs, for the 100–500 MHz frequency band. In Figure 6, the three regions, specular, diffuse, and grazing are clear to see corresponding to the angle of incidence in one of the following ranges;

$$\begin{aligned} &0 \le \vartheta \le 30^\circ, \text{ specular} \\ &30^\circ \le \vartheta \le 85^\circ, \text{ diffuse} \\ &85^\circ \le \vartheta \le 90^\circ, \text{ grazing} \end{aligned} \tag{97}$$

In the specular region, the ground clutter may mask the target return regardless of the frequency band or the target size and depth. This effect is because of the "spikey" nature of the return in the specular region. The presence of a distinct return corresponding to the target is relatively unclear from Figure 6.

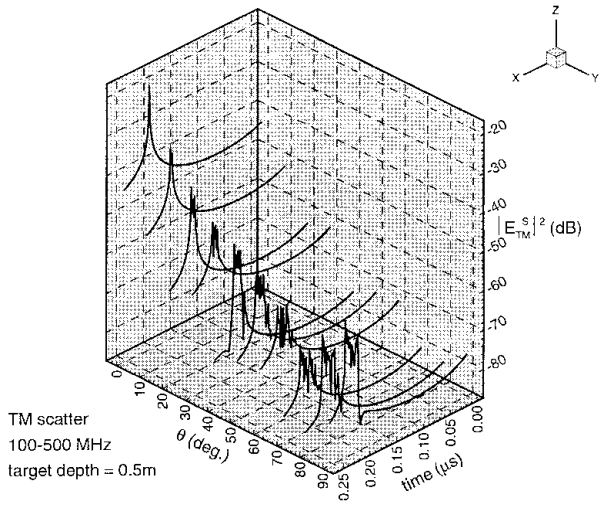

Figure 6. EM backscatter from a rough interface with the target below the interface. The polarization of the backscatter is TM and the frequency band is 100-500 MHz.

The time response in Figure 6 was obtained by performing a 256 point FFt on the frequency response. The bandwidth of the frequency response is 100 to 500 MHz giving a time step of

$$\Delta t = \frac{1}{2 \cdot 500 \cdot 10^6} = 1ns \tag{98}$$

which is also the target resolution.

Some discussion of the frequency band as it pertains to the theory used to calculate the target (i.e., ellipsoidal) scattering is needed. At the low end of the band (100 MHz) the wavelength in the medium is

$$\lambda = \frac{c/\sqrt{\varepsilon_r}}{f} \cong 0.95m \tag{99}$$

($\epsilon_r = 10$) and the semi-major dimensions for the oblate ellipsoid (a=0.1m, b=0.1m, c=0.15m) are smaller than the wavelength in

Equation (99). At the high end of the band (500 MHz) the wavelength in the medium is 0.19 m, and the target is still in the Rayleigh region. In the 300-800 MHz band where the wavelength at the high end is 0.12 m, the Rayleigh scatter is a good first order approximation to the target's scatter, and an exact solution involving a Method of Moments (MOM) approach is well beyond the scope of this study.

The complex dielectric constant of the medium was assumed to be frequency independent for all examples. In this paper however, the computation of the frequency variation of conductivity in the computer algorithm is easily modified to assume a linear variation in frequency as

$$\sigma(f) = 0.01 + \frac{\sigma_{\max}}{(f_2 - f_1)}(f - f_1) \tag{100}$$

in order to model the variation in conductivity as a function of moisture content (Scott and Smith, 1992).

Figure 7 shows the TM backscatter in the 300-800 MHz band for a target at a depth of 0.5m, and Figure 8 shows the TM response in the same band for the case of no target.

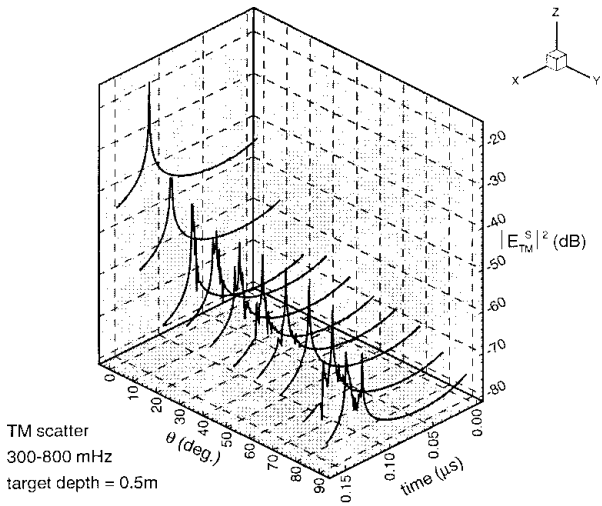

Figure 7. TM backscatter from a target buried 0.5m beneath the rough surface shown in Figure 4 in the 300-800MHz band.

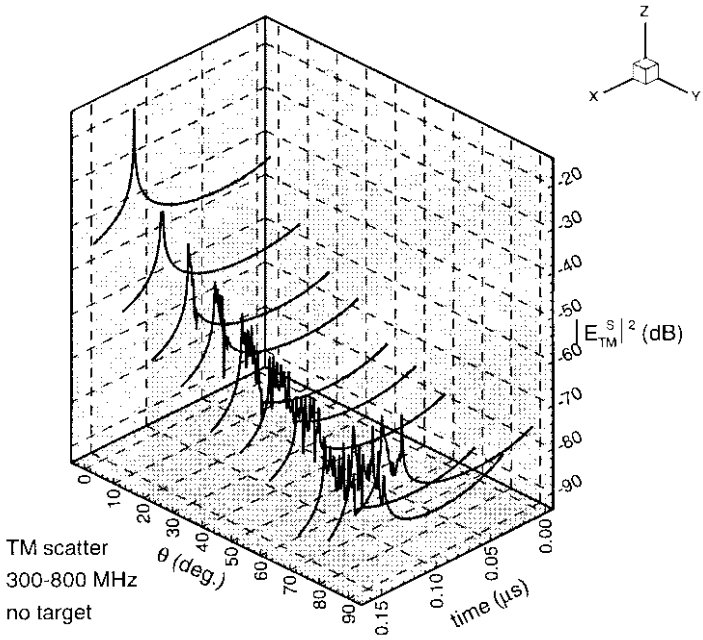

Figure 8. TM backscatter from the rough surface is shown in Figure 4 in the 300-800MHz frequency band for the case of no target.

A comparison of Figures 7 and 8 shows the occurence of a large spike in the diffuse region when the target is present, and when the target is absent, the scatter is more spikey.

In order to compare TM and TE backscatter, Figure 9 shows this case when no target is present. Again there are the three regions of scatter as described by Equation (97) with the TE return about the same strength as the TM backscatter. Because the TE component does not produce a psuedo-Brewster effect (since ϵ in medium 2 is complex, a minimum in the magnitude of the Fresnel reflection coefficient as a function of the angle on incidence) as the TM component does, the remainder of this section will only consider TM backscatter. This difference between the TM and TE components has been suggested as a technique for detection of buried objects (Baum, 1994).

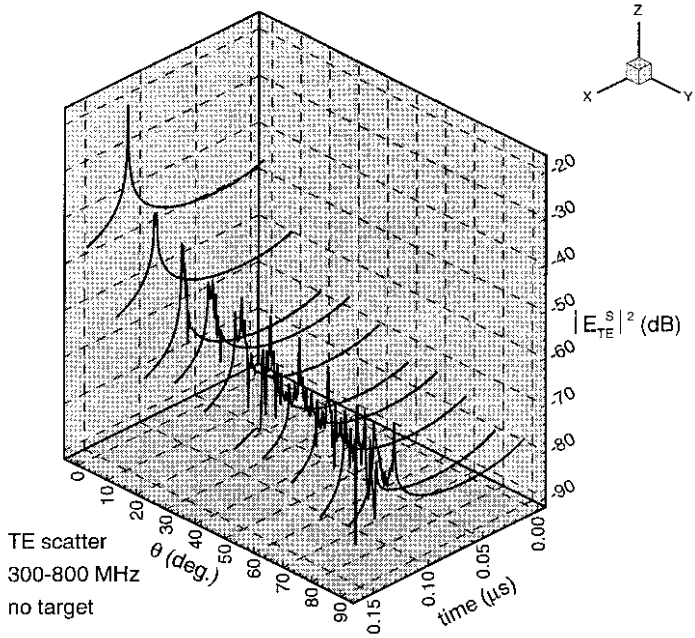

Figure 9. TE backscatter from the rough surface in Figure 5 in the 300-800 MHz frequency band for the case of no target.

In order to examine more closely the difference in the TM backscatter with and without a target present, Figure 10 shows the time response of the backscatter in the 300-800 MHz band for a specific angle of incidence, $\vartheta = 60^\circ$, for both the case of no target present and with the target present. In this frequency band, the maximum scattered power for the case with the target present is about 20 dB higher than with no target. Also, for the case of a target present, the scattered power is concentrated in a single peak, whereas with no target present, the scattered power shows several spikes.

An estimate of the time delay from the average terrain height in Figure 5 to the target 0.5m beneath the interface is given by

$$\Delta t = \frac{2d\sqrt{\varepsilon_r}}{c} = \frac{2 \cdot 0.5 \cdot \sqrt{10}}{3 \cdot 10^8} \cong 10.5ns \tag{101}$$

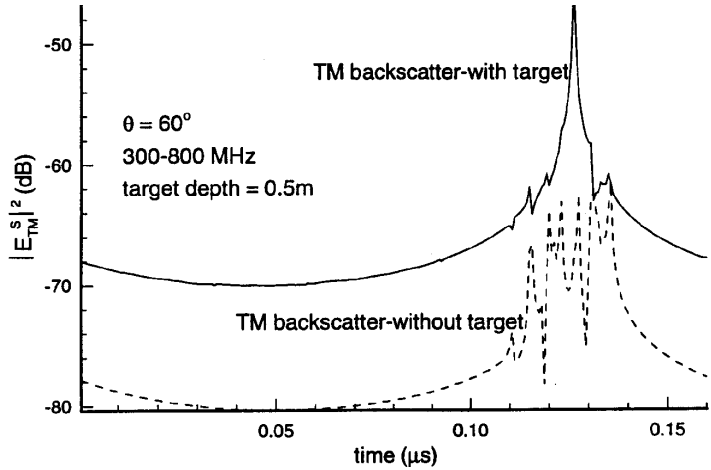

Figure 10. TM backscatter for a rough surface with and without the target present.

In Figure 10, the time delay from one of the early spikes from the interface return to the spike corresponding to the target is about

$$\delta t \cong \ .125\mu\text{s} - \ .115\mu\text{s} = 10\text{ns},$$

in good agreement with result in Equation (101).

The trade-off with frequency is best seen by considering the two bands, 100-500 MHz and 300-800 MHz using the computed clutter (interface) and target return given in Figure 10.

From the radar range equation, the received power is

$$\begin{aligned} P_r &= \frac{P_t G^2 \lambda^2 \sigma}{(4\pi)^3 R^4} \\ G &= \frac{4\pi A_e}{\lambda^2} \\ \theta_{3dB} &= \frac{\lambda}{l} \end{aligned} \tag{102}$$

and defining the time-domain characterization of radar cross-section as

$$\sigma = \frac{\int_{-\infty}^{\infty} \left(\underline{E}^{S}_{TM(TE)}(t)\right)^2 dt}{\int_{-\infty}^{\infty} \left(\underline{E}^{inc}_{TM(TE)}(t)\right)^2 dt} \tag{103}$$

and for 100–500 MHz band:

$$\begin{gathered} \text{center freq.} = 300 \text{ MHz} \\ l \text{ (antenna aperature)} = 2 \text{ m} \end{gathered}$$

and Equation (103) gives (for the case where the backscatter in Figure 10 includes the target),

$$\sigma(\vartheta = 60) = -15.08\text{dBsm}$$

and substituting into Equation (102) gives

$$\begin{aligned} \theta_{3dB} &= \frac{1}{2} \cong 28.6^\circ \\ G &= \frac{4\pi}{.25} = 50.25\ (17.0dB) \\ P_r(dB) &= 20. + 34. + 0. - 15.08 - 33.0 - 127 \\ &= -121.08dB \end{aligned}$$

By contrast, in the 300-800 MHz band,

$$\begin{aligned} \text{centerfreq.} &= 550\text{MHz} \\ \vartheta_{3dB} &= \frac{0.545}{2} \cong 15.6^\circ \\ G &= \frac{4\pi}{0.0743} = 169.2(22.3dB) \\ P_r(dB) &= 20. + 44.6 - 5.3 - 15.08 - 33. - 127. \\ &= -110.48dB \end{aligned}$$

The received clutter power is essentially the same for the two frequency bands. For $\theta = 60^\circ$, and again using Equation (103)

$$\sigma_{clutter} \cong -25.19 dBsm \tag{104}$$

and from Figure 10, the return without the target is about 16 dB below the return with the target over time duration of about 0.04μs. This corresponds to a range extent of

$$\delta r = \frac{c\delta\tau}{2} = 0.5 \times 3 \times 10^8 \times 0.04 \times 10^{-6} = 6m(7.78 dBsm).$$

Thus an alternative estimate for the clutter is

$$\begin{aligned} \sigma_{clutter}(dBsm) &\approx \sigma_{\text{target}}(dBsm) - 16dB + 7.78 dBsm \\ &\approx -15.08 - 16 + 7.78 \\ &\approx -23.3 dBsm \end{aligned} \tag{105}$$

which is reasonable agreement for the two results in Equations (104) and (105), and is in relative agreement with the land backscatter result given by Nathanson (page 320, 1991) of 28 dB for a grazing angle of 30 degrees (angle of incidence of 60 degrees), for relatively flat desert.

When the size of the footprint is calculated using the 3-dB beamwidths given above in place of the 10m by 10m patch used in the calculations corresponding to Figure 10, the size of the footprint on the ground each banc at a range R=1.5km is

$$\begin{aligned} A(100 - 500MHz) &= (\vartheta_{3dB} R)^2 = 5.625 \times 10^5 m^2 (57.5dB) \\ A(300 - 800MHz) &= 1.67 \times 10^5 m^2 (52.2dB) \end{aligned} \tag{106}$$

The normalized radar cross-section in the 300-800 MHz band for the clutter is therefore given by (from the second line in Equation (106))

$$\sigma_0(dB) = \frac{\sigma_{\text{clutter}}(dBsm)}{area(dBsm)} = -33 - 52.2 = -85.2dB \tag{107}$$

which is significantly smaller than the result in Equations (104) and (105) because, the size of the patch in Equation (106) is nearly 30 dBsm larger than the 10m by 10m square patch considered in Figure 10.

The corresponding received clutter power in the two bands is

$$\begin{aligned} P_{\text{clutter}}(100--500MHz) &= 20.+34.-25.19+57.5-33. \\ &\quad -127.=-73.7dB \\ P_{\text{clutter}}(300--800MHz) &= 20.+44.6-5.3-25.19+52.2 \\ &\quad -22.-127=-73.7dB \end{aligned} \tag{108}$$

It is interesting for these two frequency bands that the clutter power is about the same. The target-to-clutter power for the two frequency bands is

$$\begin{aligned} \left.\frac{P_r}{P_{\text{clutter}}}\right|_{100-500MHz} &\cong -47.4dB \\ \left.\frac{P_r}{P_{\text{clutter}}}\right|_{300-800MHz} &\cong -36.8dB \end{aligned} \tag{109}$$

which obviously requires some coherent integration of the received pulses (on the order of 10^6 pulses) in order to detect the target. Also from Equation (109), the clutter rejection is about the same in the two frequency bands. Equation (109) suggests that going to the higher frequency bands where and increase in antenna gain is possible may not offset the increased transmission loss versus using the HF band.

11. Concluding Remarks

This paper presents the mathematics needed to model the scattered signal from a target buried beneath an interface. Included in the derivation are: 1) the scattered field for the case where the incident field contains both a TM and a TE component with respect to the plane of incidence, 2) the motion of the source and observer with respect to the target, 3) a plane-wave spectrum representation for the scattered field in terms of the scattering matrix of the target, 4) inclusion of both the electric and magnetic dipole moments of the scattered field from the target in the medium, 5) multiple bounces in the medium between the target and the interface, and 6) a 3-D rough surface faceted model of the interface. The HF/VHF/UHF frequency band is investigated in order to determine which band is optimum for the detection of a buried

object. The tradeoff in ground penetration loss versus antenna gain for the different frequency bands is a key consideration in the design of a system used to detect buried objects. The frequency band is also an important consideration from the standpoint of the choice of amplifier, a major item in terms of cost in a practical system. Initial results indicate that the lower frequency bands will yield the higher target-to-clutter ratios, and have less transmission loss than the higher 300-800 MHz band. However, several additional examples of target size, target geometry and frequency band need to be investigated before an optimum band can be selected.

References

1. Baum, C., *Concerning the Identification of Buried Dielectric Targets,* Interaction Notes, Note 504, 24 July, 1994, Phillips Lab., Albuquerque, NM.
2. Barrick, D. E., "First-order theory and analysis of MF/HF/VHF scatter from the sea," *IEEE Trans. on Antennas and Propagation,* Vol. AP-20, 2–10, Jan. 1972.
3. Chew, W. C., *Waves and Fields in Inhomogeneous Media*, IEEE Press, New York, NY.
4. Collin, R. E., "Electromagnetic scattering form perfectly conducting rough surfaces (A new full Wave method)," *IEEE Transactions on Antennas and Propagation,* Vol. 40, No. 12, l466–1477, Dec., 1992.
5. Hill, D. A., "Electromagnetic scattering by buried objects, of low contrast," *IEEE Trans. on Geoscience and Remote Sensing* , Vol. 26, No. 2, l95–203, March, 1988.
6. Hill, D. A., and K. H. Cavcey, "Coupling between two antennas separated by a planar interface," *IEEE Trans. on Geoscience and Remote Sensing,* Vol. GE-25, No. 4, 422–431, July, 1987.
7. Ishimaru, A., *Electromagnetic Wave Propagation, Radiation, and Scattering,* p. 291, Prentice Hall, Englewood Cliffs, New Jersey, l991.
8. Kerns, D. M., *Plane-Wave Scattering Matrix Theory of Antennas and Antenna-Antenna Interaction,* NBS Monograph 162, 1981, Washington, DC.

9. Lo, Y. T., and S. W. Lee, *Antenna Handbook* , Vol. 1, "Fundamentals and Mathematical Techniques, Van Nostrand Reinhold," 3–21, 3–23, New York, 1993.
10. Nathanson, F. E., J. P. Reilly, M. N. Cohen, *Radar Design Principles,* p. 320, Second Edition, McGraw–Hill, Inc. New York, 1991.
11. Ott, R. H. , G. A. Hufford, A. Q. Howard, Jr. *Scattering by water waves generated by a moving pressure point*, *Journal of Applied Physics,* Vol. 44, No. 8, 3–21, 3–23, August, 1973.
12. Peters, L. Jr., J. J. Daniels, and J. D. Young, " Ground penetrating radar as a subsurface environmental sensing tool," *Proc. of the EEE,* Vol. 82, No. 12, 1802–1822, Dec., 1994.
13. Ruck, G. T. , D. E. Barrick, W. D. Stuart, and C. K. Krichbaum, *Radar Cross Section Handbook,* Vol. 1, Plenum Press, New York, 1970.
14. Rice, S. O., *Reflection of Electromagnetic Waves from Slightly Rough Surfaces,* in "The Theory of Electromagnetic Waves", edited by Morris Kline, 351–378, 1951.
15. Van de Hulst, H. C., *Light Scattering by Small Particles, Dover Publications,* Inc., New York, 1957.
16. Scott, W. R. and Glenn S. Smith, "Measured electrical constitutive parameters of soil as functions of frequency and moisture content," *IEEE Transactions on Geoscience and Remote Sensing,* Vol. 30, No. 3, 621–623, May, 1992.